CHAPTER 12

ESR AND MOLECULAR MOTIONS IN LIQUID CRYSTALS: MOTIONAL NARROWING

J. H. FREED, A. NAYEEM and S. B. RANANAVARE
Baker Laboratory of Chemistry
Cornell University
Ithaca
New York 14853
USA

ABSTRACT. Theoretical and experimental aspects of spin relaxation in liquid crystals are considered here, with primary emphasis on the motional narrowing regime. ESR studies of translational motion in mesophases are also described.

1. The ESR Spin Hamiltonian: g and A Tensors

The total spin hamiltonian H expressed in angular frequency units, can be separated into three components,

$$H(t) = H_0 + H_1(\Omega) + \hat{\varepsilon}(t). \tag{1}$$

In the high-field approximation the orientation independent component H_0 is:

$$\hbar H_0 = \gamma_e B_0 \hat{S}_z - \hbar \sum_i \gamma_i B_0 \hat{I}_{i,z} + \hbar \gamma_e \sum_i a_i \hat{S}_z \hat{I}_{i,z} \tag{2}$$

which gives the zeroth-order energy levels and transition frequencies. In this equation the first term is the electron spin Zeeman interaction involving the electron spin operator, $\hat{S}$, and the DC magnetic field B_0, with γ_e the electronic gyromagnetic ratio. The second term is the nuclear spin Zeeman interaction summed over all nuclei with spin operators $\hat{I}_{i,z}$ and gyromagnetic ratios γ_i. The third term is the hyperfine interaction between the electron spin and the nuclear spins and a_i is the hyperfine coupling constant. The orientation dependent part, $H_1(\Omega)$, can be expressed as the scalar product of two tensors [1], i.e.,

$$H_1(\Omega) = \sum_{\mu,i} \sum_{L,m,k} (-1)^k F'^{(L,k)}_{\mu,i} D^L_{m,-k}(\Omega) A^{(L,m)}_{\mu,i}, \tag{3}$$

$F'^{(L,k)}_{\mu,i}$ and $A^{(L,m)}_{\mu,i}$ are irreducible tensor components of rank L.The $F'^{(L,k)}_{\mu,i}$ are spatial functions in molecule fixed coordinates, while the $A^{(L,m)}_{\mu,i}$ are spin operators defined in the laboratory axis system. The subscripts μ and i refer to the type of perturbation and to the different nuclei, respectively. The generalised spherical harmonics $D^L_{mk}(\Omega)$ include the transformation from the laboratory axis system (xyz) into the molecule-fixed axis system ($x'''y'''z'''$). For the analysis of most ESR spectra of simple free radicals ($S = 1/2$) only second rank tensors are important, i.e., the A and g tensors.

For nitroxides, there are three allowed ESR transitions and six forbidden transitions which must be considered; these are illustrated in figure 1. The g tensor, **g**, and the hyperfine tensor, **A**, yield

G. R. Luckhurst and C. A. Veracini (eds.), The Molecular Dynamics of Liquid Crystals, 271–312.

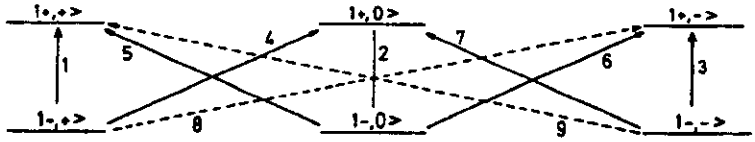

Figure 1. Energy levels and transitions for a nitroxide in high magnetic fields. Here $S=1/2$ and $I=1$, and the notation is $|M_S, M_I>$. (From [6]).

an $H_1(\Omega)$ (neglecting non-secular terms which tend to be unimportant in liquid crystals due to their relatively high viscosities) given by,

$$\begin{aligned} H_1(\Omega) &= D^2_{00}(\Omega)\left[F_0 + D'\hat{I}_z\right]\hat{S}_z + \left[D^2_{0-2}(\Omega) + D^2_{02}(\Omega)\right] \\ &\times (F_2 + D^{(2)'}\hat{I}_z)\hat{S}_z + \left[D^2_{10}(\Omega)\hat{I}_+ - D^2_{-10}(\Omega)\hat{I}_-\right]D\hat{S}_z \\ &+ \left[D^2_{12}(\Omega) + D^2_{12}(\Omega)\right]D^{(2)}\hat{I}_+\hat{S}_z \\ &- \left[D^2_{-1-2}(\Omega) + D^2_{-12}(\Omega)\right]D^{(2)}\hat{I}_-\hat{S}_z, \end{aligned} \tag{4}$$

where

$$\begin{aligned} F_i &= \sqrt{\frac{2}{3}}\, g^{(i)}\hbar^{-1}\beta_e B_0, \\ g^{(0)} &= \sqrt{\frac{1}{6}}\left[2g_{z''} - (g_{x''} + g_{y''})\right], \\ g^{(2)} &= \frac{1}{2}[g_{x''} - g_{y''}], \\ D &= (|\gamma_e|/2\sqrt{6})(A_{x''} + A_{y''} - 2A_{z''}), \\ D^{(2)} &= \frac{1}{4}|\gamma_e|(A_{y''} - A_{z''}), \end{aligned} \tag{5}$$

$D' = -(8/3)^{1/2}D$ and $D^{(2)'} = -(8/3)^{1/2}D^{(2)}$. We have written the principal components of the hyperfine tensor, $A_{x''}, A_{y''}, A_{z''}$ and those of the g tensor $g_{x''}, g_{y''}, g_{z''}$ in the molecular coordinate frame $(x''' y''' z''')$ in which they are diagonal. In addition,

$$\hat{\varepsilon}(t) = \frac{1}{2}\gamma_e B_1\left[\hat{S}_+ \exp(-i\omega t) + \hat{S}_- \exp(i\omega t)\right] \tag{6}$$

is the interaction of the electron spin with an oscillating magnetic field of frequency $\omega/2\pi$. [When more than one oscillating field, (i.e., for such double resonance techniques as ELDOR or ENDOR,

and/or when field modulation effects are to be explicitly incorporated), then equation (6) may be appropriately modified to include these effects.]

1.1. ANISOTROPIC LIQUIDS

Suppose now that the liquid has a preferred axis of orientation, i.e., the director. We now write the perturbing hamiltonian (3) as

$$H_1(\Omega,\Psi) = \sum_{\mu,i} \sum_{L,m,m',k} (-1)^k \; D^L_{m,m'}(\Psi)\, D^L_{m',-k}(\Omega)\, F'^{L,k}_{\mu,i}\, A^{L,m}_{\mu,i}. \tag{7}$$

This equation is based on two sets of rotations of the coordinate systems, first from the laboratory axis system (xyz) into the director axis system (x″y″z″) with Euler angles Ψ and then into the molecular axis system (x′y′z′) with Euler angles $\Omega(\equiv \alpha\beta\gamma)$. The orientation of the director relative to the laboratory frame can be specified by the two polar angles θ' and φ' such that $\Psi = (0,\theta',\varphi')$. More precisely, we mean by the molecular coordinate system (x′ y′ z′) the principal axis system for the orientation of the molecule in the mesophase, which is usually taken by symmetry to correspond to the principal axes of **R**, the rotational diffusion tensor. It may also be necessary to transform from the principal axis system of the magnetic interactions (x‴y′z‴) to the (x′y′z′) system with Euler angles $\Theta(\equiv \alpha'\beta'\gamma')$ according to

$$F'^{L,k}_{\mu,i} = \sum_{k'} D^L_{k',k}(\Theta)\, F'''^{L,k'}_{\mu,i}. \tag{8}$$

2. Effective Spin Hamiltonian and Order Parameters

In ordered systems, an effective spin hamiltonian is used

$$H = H'_0 + H'_1(\Omega), \tag{9}$$

where

$$H'_0 = H_0 + \langle H_1(\Omega) \rangle \tag{10}$$

and

$$H'_1(\Omega) = H_1(\Omega) - \langle H_1(\Omega) \rangle, \tag{11}$$

where the averaging implied by the angular brackets is over ensemble variables (i.e., the space of Euler angles describing the relative orientation of the molecule in the laboratory frame). Thus, from equation (7) we have for uniaxial liquid crystals

$$\langle H_1(\Omega) \rangle = \sum_{L,k,m,\mu,i} (-1)^k\, D^L_{m,0}(\Psi) \langle D^L_{0,-k}(\Omega) \rangle\, F'^{L,k}_{\mu,i}\, A^{L,m}_{\mu,i}. \tag{12}$$

The solution of this hamiltonian is formally identical to that for a single crystal hamiltonian with axially symmetric magnetic parameters, i.e., for a single nucleus such as ^{14}N

$$\tilde{F}^{(L,0)}_{\mu} = \sum_{k} (-1)^k \langle D^L_{0,-k}(\Omega) \rangle\, F'^{(L,k)}_{\mu}. \tag{13}$$

Thus,

$$\tilde{a}_{\parallel} = a_N + \sqrt{\frac{2}{3}} \sum_k 2\pi \xi_N D_N^{(k)} (-1)^k \langle D^2_{0,-k}(\Omega) \rangle, \tag{14}$$

$$\tilde{a}_{\perp} = a_N - \sqrt{\frac{1}{6}} \sum_k 2\pi \xi_N D_N^{(k)} (-1)^k \langle D^2_{0,-k}(\Omega) \rangle, \tag{15}$$

where $\xi_N D_N^{(k)}$ are the irreducible components of the hyperfine tensor, and

$$\tilde{g}_{\parallel} = g_e + \sqrt{\frac{2}{3}} \sum_k g^{(k)} (-1)^k \langle D^2_{0,-k}(\Omega) \rangle, \tag{16}$$

$$\tilde{g}_{\perp} = g_e - \sqrt{\frac{1}{6}} \sum_k g^{(k)} (-1)^k \langle D^2_{0,-k}(\Omega) \rangle, \tag{17}$$

with $g^{(k)}$ the irreducible components of the g tensor. We may write

$$\langle g \rangle = \tilde{g}(\theta) \equiv (\tilde{g}_{\parallel}^2 \cos^2 \theta + \tilde{g}_{\perp}^2 \sin^2 \theta)^{1/2}, \tag{18}$$

and when the g values deviate only slightly from g_e we can write

$$\langle a \rangle = \tilde{a}(\theta) \equiv (\tilde{a}_{\parallel}^2 \cos^2 \theta + \tilde{a}_{\perp}^2 \sin^2 \theta)^{1/2} \tag{19}$$

then the resonant field is given by:

$$\begin{aligned} B(\theta) \simeq g_e B_0 \left(2 - \frac{\tilde{g}(\theta)}{g_e}\right) - \tilde{a}(\theta) M_N - \frac{\left(\tilde{a}_{\parallel}^2 + \tilde{a}(\theta)^2\right) \tilde{a}_{\perp}^2}{4\tilde{a}(\theta)^2} \left[I(I+1) - M_N^2\right] \\ \times \left[3 - 2\frac{\tilde{g}(\theta)}{g_e}\right] - M_N^2 \left[\frac{(\tilde{a}_{\perp}^2 - \tilde{a}_{\perp}^2)^2}{8\tilde{a}(\theta)^2 B_0}\right] \left[3 - 2\frac{\tilde{g}(\theta)}{g_e}\right] \sin^2 2\theta. \end{aligned} \tag{20}$$

When the ordering is weak and when $\langle D^2_{00}(\Omega) \rangle_{z'}$ and $\langle D^2_{02} + D^2_{0-2} \rangle_{z'}$ are non-zero these equations simplify to

$$\begin{aligned} B(\theta) \simeq B_0 \left(2 - \frac{\langle g \rangle}{g_e}\right) - \langle a \rangle M_N - \frac{a_N^2}{2B_0} \left[I(I+1)\right] \\ - M_N^2 \left[1 - \left(\frac{\langle a \rangle}{a_N} - 1\right) 2 \left(\frac{\langle g \rangle}{g_e} - 1\right)\right]. \end{aligned} \tag{21}$$

The apparent g and a values, i.e., $\langle g \rangle$ and $\langle a \rangle$ may then be used to obtain the order parameters $\langle D^2_{00} \rangle$ and $\langle D^2_{02} + D^2_{0-2} \rangle$ according to

$$<D^2_{00}> = \frac{(<a> - a)(g_x - g_y) - (<g> - g)(a_x - a_y)}{D^2_{00}(0,\theta,0)\left[(a_z - a)(g_x - g_y) - (g_z - g)(a_x - a_y)\right]} \tag{22}$$

and

$$<D^2_{02} + D^2_{0-2}> = \frac{\sqrt{6}(<a> - a)(g_z - g) - (<g> - g)(a_z - a)}{D^2_{00}(0,\theta,0)\left[(a_z - a)(g_x - g_y) - (g_z - g)(a_x - a_y)\right]}, \tag{23}$$

where θ is the angle between director and the external magnetic field B_0 and

$$D^2_{00}(0,\theta,0) = (3\cos^2\theta - 1)/2. \tag{24}$$

[In equation (11) and hereafter we shall refer to magnetic tensor components in the x‴,y‴,z‴ axes as the x,y,z components, or else some cyclic permutation of the (x‴,y‴,z‴) axes provided there is no confusion with the laboratory axes.]

3. Spectral Densities and Linewidths

Spin relaxation in the motional narrowing regime is determined by the reduced correlation function

$$<H_1(\Omega,t)\,H_1^*(\Omega_0,t = 0)> - <H_1(\Omega)><H_1^*(\Omega_0)>, \tag{25}$$

where $H_1(\Omega)$ is the time dependent part of the spin hamiltonian. Since the time dependence of $H_1(\Omega)$ is then carried entirely by the $D^2_{m,-k}(\Omega)$ for weak ordering [or coincident laboratory (x,y,z) and director (x‴,y‴,z‴) axes] (see later), we need only consider the correlation functions of the $D^2_{m,-k}(\Omega)$ given by

$$C_{m,m',-k,-k'}(t) = <D^{(2)}_{m,k}(\Omega)\,D^{(2)*}_{m',k'}(\Omega_0)> - <D^{(2)}_{m,k}(\Omega)><D^{(2)*}_{m',k'}(\Omega_0)>. \tag{26}$$

The spectral densities are Fourier-Laplace transforms of these correlation functions, i.e.,

$$j_{m,m',k,k'}(\omega) = \mathrm{Re}\int_0^\infty dt\, C_{m,m',k,k'}(t)\, e^{-i\omega t}\,\delta_{m,m'}, \tag{27}$$

where $\delta_{m,m'}$ appears because for a uniaxial phase $m = m'$. Although the fundamental spectral densities important for spin relaxation are indeed given by equations (26) and (27), it is convenient to define spectral densities directly from equations (3) and (25) for ease of relating to observables. Thus we obtain the measurable spectral density

$$J^{\mu\nu}_m(\omega) = \sum_{k,k'} F'^{2,k}_{\mu}\, F'^{2,k'*}_{\nu}\, j_{m,m',k,k'}(\omega)\,\delta_{m,m'}, \tag{28}$$

where μ and ν indicate the magnetic tensors associated with the particular interactions.

In general the spectral densities of equation (27) are derived from a stochastic time evolution operator Γ via the resolvent

$$j_{m,m',k,k'}(\omega) = \mathrm{Re}\{< \delta D^2_{mk} \mid (i\omega + \Gamma)^{-1} \mid P\,\delta D^2_{m'k'} >\}, \tag{29}$$

where P is the unique equilibrium probability distribution obeying the relation

$$\Gamma P = 0 \tag{30}$$

and the bra $< \delta D^2_{mk} \mid$ is defined by

$$< \delta D^2_{mk} \mid \Omega > \equiv D^2_{mk}(\Omega) - < D^2_{mk}(\Omega) >. \tag{31}$$

Thus δD^2_{mk} denotes the deviation from the thermal average $< D^2_{mk} >$. In the following sections the spectral densities are given explicitly or they are derived from a stochastic operator Γ utilising equation (29).

For a single nucleus of spin I we have for the dependence of T_2 on the z component of nuclear spin, M_I

$$T_2(M_I)^{-1} = A + BM_I + CM_I^2, \tag{32}$$

where

$$\begin{aligned} A - A' = {} & \frac{1}{3} I(I+1)\,\gamma_e^2 \sum_{k,k'} D_k D_{-k'} \{j_{0,k,k'}(\omega_e) + 3j_{1,k,k'}(\omega_a) + 6j_{2,k,k'}(\omega_e)\} \\ & + \frac{\hbar^2 \gamma_e^2}{16\beta_e^2} \sum_{k,k'} F_k F_{-k'} \{4j_{0,k,k'}(0) + 3j_{1,k,k'}(\omega_e)\} \end{aligned} \tag{33}$$

$$B = -\frac{\hbar\gamma_e^2}{\sqrt{6}\,\beta_e} \sum_{k,k'} D_k F_{-k'} \{4j_{0,k,k'}(0) + 3j_{1,k,k'}(\omega_e)\} \tag{34}$$

$$C = \frac{\gamma_e^2}{3} \sum_{k,k'} D_k D_{-k'} \{8j_{0,k,k'}(0) - j_{0,k,k'}(\omega_e) + 6j_{1,k,k'}(\omega_e) - 3j_{1,k,k'}(\omega_a) - 6j_{2,k,k'}(\omega_e)\} \tag{35}$$

where the D_k and F_k are the spherical tensor components of the electron-nuclear dipolar and Zeeman tensors in the diffusion tensor principal axis system (x',y',z'), and where $\omega_a = (1/2)\,a \mid \gamma_e \mid \pm\omega_n$, with ω_n the nuclear Larmor frequency. For the case of perdeuteriated tempone-d_{16}, the y axis of the magnetic tensor principal axis system is coincident with the z' axis of the diffusion tensor principal axis system, and the probe is said to be y ordered. In terms of measurable spectral densities (cf. equation (28)) we obtain

$$A - A' = 2J_1^{DD}(\omega)_a + (2/3)J_0^{DD}(\omega_e) + 4J_2^{DD}(\omega_e) + (8/3)J_0^{GG}(0) + 2J_1^{GG}(\omega_e) \tag{36}$$

$$B = (16/3)J_0^{DG}(0) + 4J_1^{DG}(\omega_e) \tag{37}$$

$$C = (8/3)J_0^{DD}(0) - J_1^{DD}(\omega_d) + 2J_1^{DD}(\omega_e) - (1/3)J_0^{DD}(\omega_e) - 2J_2^{DD}(\omega_e) \tag{38}$$

A' in equations (33) and (36) includes all other nuclear spin independent line broadening mechanisms, which for homogeneous T_2's is predominantly spin rotation [5] for low concentrations of probe, whereas Heisenberg spin exchange becomes important for higher concentrations [6]. For the nuclear spin transition rate $2W_n$ we have

$$2W_n = J_1^{DD}(\omega_d) = \gamma_e^2 \sum_{k,k'} (D_k D_{-k'}) j_{1,k,k'}(\omega_d) \tag{39}$$

and for the terms involving electron spin transitions we obtain [6]

$$W_e(M_1) = W_e^{SR} + 2J_1^{GG}(\omega_e) + 4J_1^{DG}(\omega_e)M_1 + 2J_1^{DD}(\omega_e)M_1^2, \tag{40}$$

$$W_{x_1} = (2/3)J_0^{DD}(\omega_e), \tag{41}$$

$$W_{x_2} = 4J_2^{DD}(\omega_e), \tag{42}$$

where W_{x_1} and W_{x_2} are the cross-relaxation rates associated with $S_z I_z$ and $S_z I_z$, respectively.

Equations (33-42) are applicable when the director is aligned parallel to the magnetic field. If the director is rotated by an angle θ with respect to the field we obtain

$$\hat{j}_{m,k,k'}(\omega,\theta) = \sum_{m'=-2}^{+2} | d^{(2)}_{m',m}(\theta) |^2 j_{m,k,k'}(\omega), \tag{43}$$

or alternatively

$$\hat{J}_m^{\mu\nu}(\omega,\theta) = \sum_{m'=-2}^{+2} | d^2_{m',m}(\theta) |^2 J_{m'}^{\mu\nu}(\omega), \tag{44}$$

where the $d^2_{m',m}(\theta)$ are the reduced Wigner rotation matrix elements of rank two, which can be evaluated in terms of their Clebsch-Gordan series expansions [7],

$$| d^2_{m',m}(\theta) |^2 = (-1)^{m'-m} \sum_{L=0,2,4} C(2,2,L;m,-m)\, C(2,2,L;m',-m')\, d^L_{00}(\theta). \tag{45}$$

The spectral densities in equation (44) have the property [5] that

$$J_m^{\mu\nu}(\omega) = J_{-m}^{\mu\nu}(\omega) \tag{46}$$

and hence the angular dependence of $\hat{J}_m^{\mu\nu}(\omega,\theta)$ is fully described by the spectral densities $J_0^{\mu\nu}(\omega)$, $J_1^{\mu\nu}(\omega)$, and $J_2^{\mu\nu}(\omega)$. In this version of the motional-narrowing theory, the ^{14}N spin is assumed to be quantised along the laboratory z axis. Luckhurst and Zannoni [8] point out that the form of equation (44) is accurate only when the orientational ordering of the probe is weak ($S < 0.3$), such that the axis of ^{14}N spin quantisation does not deviate substantially from the laboratory z axis. Thus we have for the orientation dependent $J_m(\omega,\theta)$ in the case of weak probe ordering:

$$J_0(\omega,\theta) = (1/4)(1-3\cos^2\theta)^2 J_0(\omega) + 3\cos^2\theta\sin^2\theta J_1(\omega) + (3/4)\sin^4\theta J_2(\omega) \quad (47)$$

$$J_1(\omega,\theta) = (3/2)\cos^2\theta\sin^2\theta J_0(\omega) + (1/2)\left[(1-2\cos^2\theta)^2 + \cos^2\theta\right] J_1(\omega) + (1/2)(1-\cos^4\theta) J_2(\omega) \quad (48)$$

$$J_2(\omega,\theta) = (3/8)\sin^4\theta J_0(\omega) + (1/2)(1-\cos^4\theta) J_1(\omega) + (1/8)\left[(1+\cos^2\theta)^2 + 4\cos^2\theta\right] J_2(\omega). \quad (49)$$

Thus for example, for $2W_n(\theta)$ we have:

$$2W_n(\theta) = (3/2)\cos^2\theta\sin^2\theta J_0^{DD}(\omega_a) + (1/2)\left[(1-2\cos^2\theta)^2 + \cos^2\theta\right] J_1^{DD}(\omega_a) + (1/2)(1-\cos^4\theta) J_2^{DD}(\omega_a). \quad (49)$$

Thus the orientation dependent spin relaxation rates such as the $W_n(\theta)$ yield with the application of equations (47-49) the three spectral densities $J_0^{DD}(\omega)$, $J_1^{DD}(\omega)$ and $J_2^{DD}(\omega)$. We will see in the following sections that an experimental determination of these three spectral densities allows for a much closer comparison of theoretical models of the dynamics with experiment than is possible without the orientation dependent data.

4. Rotational Dynamics in Liquid-Crystalline Phases

The diffusion of a solute molecule in a liquid-crystalline environment is influenced by the orienting potential as described in Chapters 3 and 4. However, since in liquid crystals several kinds of motions may occur simultaneously (those occuring at the molecular level, i.e., rotations, translations and conformational changes, as well as those that involve large numbers of molecules leading to collective motions and order fluctuations), the dynamics is considerably more complicated than in simple isotropic liquids. In contrast to the latter, the environment of the spin probe is highly anisotropic even though the rate of molecular reorientation may be fast. The linewidths depend on both the rotational correlation time as well as on the ordering. Changes in the activation energy for rotational motion can reflect the changes in the dynamic molecular structure experienced by the probe molecule as the liquid crystal undergoes phase transitions. A chart summarising the various models for rotational diffusion appears as table 1.

4.1. MAGNETIC PARAMETERS

The relaxation data obtained from ESR studies of spin probes in liquid crystals, such as linewidths and line shifts, require an accurate knowledge of the g and A tensors of the probe in the solvent in order to obtain information leading to order parameters and rotational correlation times [9]. Although the magnetic tensors are most commonly obtained through simulations of the rigid limit spectra, cooling the liquid crystal to the rigid limit may freeze-in some order, and therefore a truly isotropic powder spectrum may not be obtained. Furthermore, the isotropic values of the g and

Table 1. Summary of Rotational Relaxation Mechanisms. [From D.J.Schneider and J.H.Freed, in "Lasers, Molecules and Methods", J.O.Hirschfelder, R.E.Wyatt, R.D.Coalson, Eds. John Wiley & Sons, New York (1989), Chapter 10].

	Mechanism	Characteristic	Parameters
1	Anisotropic diffusion	Unequal reorientation rates about principal axis system fixed in molecule; when reorientation rates are equal, this becomes isotropic brownian diffusion.	$D_R^{\parallel} = (6\tau_R^{\parallel})^{-1}$ rotational diffusion coefficients about molecular symmetry axis; $D_R^{\perp} = (6\tau_R^{\perp})^{-1}$ rotational diffusion coefficient about molecular axes perpendicular to symmetry axis; $N = \tau_R^{\perp}/\tau_R^{\parallel}$
2	Anisotropic viscosity	Unequal reorientation rates about principal axis system fixed in laboratory (i.e., dc magnetic field axis)	$\hat{D}_R^{\perp} = (6\hat{\tau}_R^{\parallel})^{-1}$ rotational diffusion coefficient about orienting axis in laboratory frame; $\hat{D}_R^{\perp} = (6\hat{\tau}_R^{\perp})^{-1}$ rotational diffusion coefficient perpendicular to orienting axis in laboratory frame; $\hat{N} = \hat{\tau}_R^{\perp}/\hat{\tau}_R^{\parallel}$
3	Fluctuating torques	Anisotropic torques that induce reorientation are themselves relaxing at rate that is not much faster than reorientation of probe molecule	τ_R = relaxation time for rotational diffusion of probe molecule; τ_M = relaxation time for fluctuating torques inducing reorientation of probe molecule; $\varepsilon \equiv (1 + \tau_M/\tau_R)^2$; may be combined with analogues of models 1 (requiring additional specification of $\tau_M^{\parallel}$ and $\tau_M^{\perp}$) or 2 (requiring $\hat{\tau}_M^{\parallel}$ and $\hat{\tau}_M^{\perp}$)
4	SRLS	Probe molecule relaxes in local potential field, while latter averages out isotropically at significantly slower rate than rate of probe molecule reorientation	$S_1 = \langle P_2(\cos\theta)\rangle$ order parameter of probe relative to local anisotropic potential field (i.e., local structure); τ_s = relaxation rate of local structure (may also be combined with analogues of models 1 or 2)
5	Jump diffusion	Molecule reorients by random jumps of arbitrary angle	$D = (\varepsilon^2)_{av}/6\tau$, where τ = time between jumps and $(\varepsilon^2)_{av}$ = mean-square jump angle; can be generalised to include anisotropic diffusion tensors by analogy with models 1 or 2

Table 1. Continued

	Mechanism	Characteristic	Parameters
6	Free diffusion	Molecular reorientation is partially due to free gaslike motion that is perturbed by frictional effects of surroundings	τ_R and τ_f, where τ_f = angular momentum relaxation time; they are often related by the Hubbard-Einstein relation; $\tau_R\tau_f = I/6k_BT$, I = moment of inertia; also, $\tau_f^{-1} = \beta$, friction coefficient
7	Director fluctuations	Hydrodynamic effect in which nematic director fluctuates in its orientation with respect to applied magnetic field	$\tau_q^{-1} = Kq^2/\eta$, where τ_q = relaxation time of qth Fourier component of director fluctuation, with K = average elastic constant of liquid crystal and η = viscosity
8	Critical fluctuations	Pretransitional effects near (almost) second/ order phase transition; leads to apparent divergences in spin relaxation due to divergences in correlation length and/or relaxation time for order parameter.	$\tau_q^{-1} = \omega_\xi(I + q^2\xi^2)^x$, where, for isotropic-nematic (nematic-smectic) transitions, $\omega_\xi = L/\nu\xi$, with L = force constant for order fluctuations and ν = associated viscosity ($\omega_\xi = \tau_m^{-1}$, with τ_m = relaxation time of smectic clusters), ξ = coherence length of nematic (smectic) order fluctuations and $x = 1(3/4)$
9	Discrete Jumps	Molecule reorients by discrete jumps among equivalent sites; often this reorientation is about single internal axis	τ_{df} = mean time between jumps

A tensors depend on the polarity of the solvent [3,10]. Since the location of the probe in the liquid crystal varies from phase to phase (as discussed later), we find that the isotropic values of g and A can be different in different phases of the liquid crystal [3]. For these reasons, the magnetic tensors measured at the rigid limit may not necessarily correspond to the correct values.

A convenient method that circumvents the need for cooling the liquid crystal to the rigid limit involves the method of scaling the magnetic tensors [3,10]. This method is based on the noted linear correlation that exists between the isotropic hyperfine splitting a_N and the solvent polarity as shown in figure 2 and discussed in detail elsewhere [3,10]. It makes use of the assumption that the components of the A and g tensors scale in the same way as the isotropic a_N and g shifts (i.e., $g_s - g_e \equiv \Delta g_s$, where g_e is the free electron g factor), i.e.,

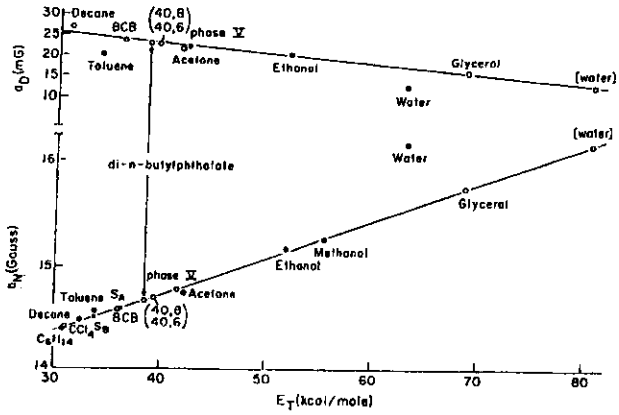

Figure 2. Variation of hyperfine splittings A_N and A_D for perdeuteriated tempone with E_T, the molar transition energy. (From [10]).

$$A_{ii}^{x}/a_{N}^{x} = A_{ii}^{0}/a_{N}^{0}, \qquad i = \text{x, y or z}$$

and

$$g_{ii}^{x}/\Delta g_{s}^{x} = g_{ii}^{0}/\Delta g_{s}^{0}.$$

In these equations, the superscript x denotes the liquid crystal whose magnetic tensors are not known (but the isotropic values Δg_s^0 and a_N^0 are known), whereas the superscript 0 indicates the same variables for the liquid crystal in which the parameters have been reliably measured. It is found that the variation in g and A values for a given probe in different liquid crystal solvents is small (10% at the very most), and therefore the linear scaling is reasonable. Indeed, the method of scaling to obtain the magnetic tensors for analysis has been used quite routinely after having been checked in several instances [3,11,13,14]. Table 2 shows the magnetic tensors for perdeuteriated tempone-d_{16} in several liquid crystals.

Table 2. Magnetic parameters for spin probes in 6OCB-8OCB and 4O.6. (From [3, 11 and 14]).

Probe	Solvent	$g_{x'}$	$g_{y'}$	$g_{z'}$	$A_{x'}/G$	$A_{y'}/G$	$A_{z'}/G$
PD-Tempone	6OCB-8OCB	2.0099	2.0062	2.00215	5.60	5.00	33.65
MOTA	6OCB-8OCB	2.0099	2.0064	2.0023	5.92	5.29	35.6
PD-Tempone	4O.6	2.0099	2.0062	2.00215	5.57	4.98	33.49
MOTA	4O.6	2.0099	2.0064	2.0023	5.89	5.26	35.41
P-probe	4O.6	2.0094	2.0058	2.0026	7.32	7.82	31.50

4.2. RELAXATION PARAMETERS: LINEWIDTHS AND LINE POSITIONS

The ESR spectra of perdeuteriated tempone-d_{16} in liquid crystals usually lie in the motional narrowing region. The intrinsic linewidths are obtained by deconvoluting the observed lineshape, which is treated as a superposition of 25 superhyperfine lines separated by a_D, the deuterium hyperfine coupling constant. A detailed description of this deconvolution procedure can be found elsewhere (cf. figure 3 in [3]). The linewidth coefficients A, B and C are obtained from equation (32). Note that while A is the intrinsic width of the central hyperfine line, B and C are (mean) differences of intrinsic widths; therefore, if there are sources of inhomogeneous broadening other than the superhyperfine contribution (i.e., magnetic field inhomogeneity), they usually affect the A term more significantly than B or C (but see later). We also note that the error bars associated with measurements of A tend also to be much larger than those for B and C. The variation of these parameters with temperature is Arrhenius-like away from phase transitions as they reflect the rotational dynamics of the probe. However, near phase transitions their variation is anomalous, and this is related to fluctuations in the order parameter of the liquid crystal. This matter is discussed in depth in Chapter 14.

ACRONYM	NAME	STRUCTURE
P-probe	2-2'-6-6'-tetramethyl 4-(butyl-oxy)-benzoyl-amino piperidine 1-oxyl; (perdeuterated piperidine ring)	
PDT	2,2,6,6-tetramethyl-4-piperidine N-oxide; (perdeuterated)	
stearamide probe	(4-octadecanoyl) amino-2,2',6,6'-tetramethyl piperidinyl-1-oxy	
CSL	3',3'-dimethyloxazolidinyl-N-oxy 2',3-5α-cholestane	
EOTA	4-ethyl amino-2,2,6,6-tetra-methylpiperidinyl-1-oxy	

Figure 3. Structures of spin probes used in our study. (From [11]).

In addition to measuring A, B and C, the shifts in the positions of the three hyperfine lines, or more particularly, the variations in the mean hyperfine splittings and g shifts with temperature are recorded since they relate to the ordering of the probe (cf. equations (22) and (23)). We typically note that ordering increases on lowering the temperature, especially at the N-I transition there is a sudden increase in ordering from the isotropic value of zero. Upon lowering the temperature within the N phase, the ordering increases and gradually levels off. It does not appear to show any abrupt changes at second order S_A-N transitions (i.e., for 4-n-butyloxybenzylidene-4-n-hextylaniline (4O.6) or 4-n-octyl-4'-cyanobiphenyl (8CB).

Examples of the variations of the linewidth coefficients and order parameters with temperature are now discussed.

4.3. MOLECULAR MOTIONS IN LIQUID-CRYSTALLINE PHASES

Here we shall discuss the rotational dynamics of perdeuteriated tempone-d_{16}, whose structure is shown in figure 3, in a variety of liquid crystal solvents including 4O.6, 4O.8, 8CB, Phase V and

6OCB-8OCB, in order to illustrate the range of information that can be obtained about the dynamic molecular structure of mesophases from motional-narrowing relaxation studies. Figure 4 shows the structures and phase transition temperatures of the liquid crystals studied here. Examples of the use of larger probes, which typically show slow-motional ESR spectra in liquid-crystalline solvents, are reserved for Chapter 15.

ACRONYM	NAME	STRUCTURE
40, 6	N-(p-butoxybenzylidene)-p-n-hexylaniline	$C_4H_9-O-C_6H_4-CH=N-C_6H_4-C_6H_{13}$
40, 8	N-(p-butoxybenzylidene)-p-n-octylaniline	$C_4H_9-O-C_6H_4-CH=N-C_6H_4-C_8H_{17}$
8CB	4-cyano-4'-octylbiphenyl	$N\equiv C-C_6H_4-C_6H_4-C_8H_{17}$
5CB	4-cyano-4'-n-pentyl biphenyl	$N\equiv C-C_6H_4-C_6H_4-C_5H_{11}$
S2	Eutectic mixture of: 4-cyano-4'-n-octyl biphenyl; 4-cyano-4'-n-decyl biphenyl; 4-cyano-4'-n-decyl oxy biphenyl	$C_8H_{17}-C_6H_4-C_6H_4-C\equiv N$ 50%; $C_{10}H_{21}-C_6H_4-C_6H_4-C\equiv N$ 39%; $C_{10}H_{21}O-C_6H_4-C_6H_4-C\equiv N$ 11%
phase V	eutectic mixture of four compounds	$C_4H_9-\phi-N(\rightarrow O)=N-\phi-OCH_3$ (25%); $C_4H_9-\phi-N=N(\rightarrow O)-\phi-OCH_3$ (40%); $C_2H_5-\phi-N(\rightarrow O)=N-\phi-OCH_3$ (12%); $C_2H_5-\phi-N=N(\rightarrow O)-\phi-OCH_3$ (22.6%)
TBBA	terephalylidene-bis-4-n-butylaniline	$C_4H_9-\phi-N=CH-\phi-CH=N-\phi-C_4H_9$

Figure 4. Some liquid crystals used in our studies. (From [11]).

Figures 5a-5e show the temperature variation of τ_R for perdeuteriated tempone-d_{16} in some liquid crystals, while the results in table 3 summarises the activation energies and pre-exponential factors associated with the rotational correlation times of perdeuteriated tempone-d_{16} in these solvents. The results for each common phase for the liquid crystals will be discussed individually in order to present a unified picture of the dynamics within that phase. We shall then attempt to provide a model for the change in probe dynamics as the phase of the liquid crystal is altered.

a.

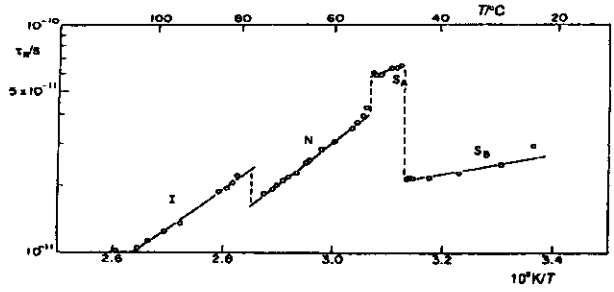

b.

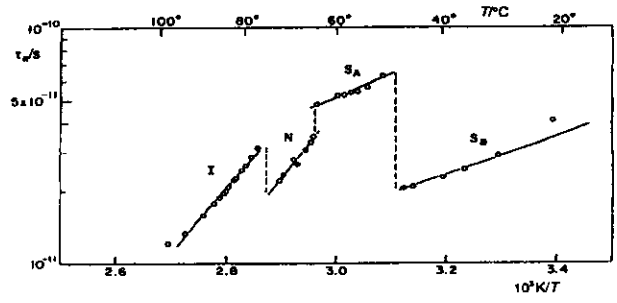
100°
80°
60°
40°
T/°C
20°
τ_R/s
5×10^{-11}
10^{-11}
I
N
S_A
S_B
2.6
2.8
3.0
3.2
3.4
10^3K/T

c.

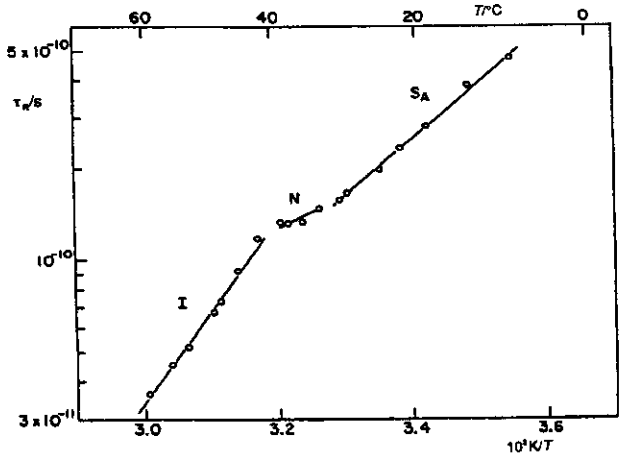
60
40
20
T/°C
0
5×10^{-10}
τ_R/s
10^{-10}
3×10^{-11}
I
N
S_A
3.0
3.2
3.4
3.6
10^3K/T

d.

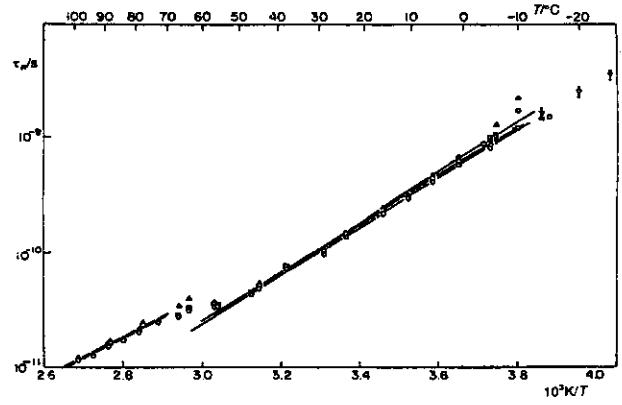
100 90 80 70 60 50 40 30 20 10 0 -10 T/°C -20
τ_R/s
10^{-9}
10^{-10}
10^{-11}
2.6
2.8
3.0
3.2
3.4
3.6
3.8
4.0
10^3K/T

e.

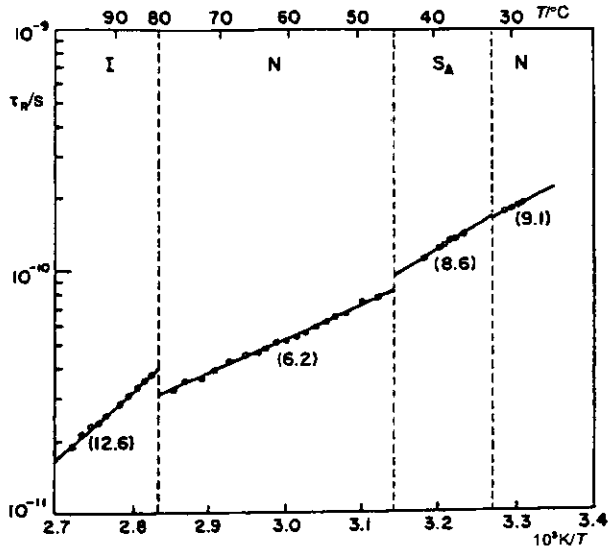

Figure 5. τ_R versus $1/T$ for perdeuteriated tempone in (a) 4O.6; (b) 4O.8; (c) 8CB; (d) Phase V; (e) 6OCB-8OCB, with ΔE_{act} indicated in parentheses. (From [3]); (d) See [5]. The points given by open circles represent the best fit obtainable for an axial potential allowing for anisotropic viscosity. The results for an asymmetric potential with anisotropic rotation (△) and with anisotropic viscosity (□) are also shown; (e) See [14].

4.3.1. *Isotropic Phase.* The linewidth results for perdeuteriated tempone-d_{16} in the isotropic phases show that, since the rotational correlation times lie between 10 to 100 ps (see figure 5), we are in the region $\omega_0^2 \tau_R^2 \geq 1$ where non-secular terms are not negligible. (Note that for conventional ESR at 9 GHz, ω_0^{-1} = 17 ps). If non-secular terms are included in the calculation of τ_R, we find that τ_R determined from B does not equal τ_R from C for isotropic rotation. Such behaviour has been commonly observed [5,3] in the region where $\omega_0^2 \tau_R^2 \sim 1$, and was fitted by modifying the spectral density function for the non-secular terms. That is, the quantity $\tau_R/(1 + \omega^2 \tau_R^2)$ is changed to $\tau_R/(1 + \varepsilon\omega^2 \tau_R^2)$ where ε is an adjustable parameter greater than unity. The rationale for employing a non-Debye-like spectral density can be understood in terms of the fluctuating torques model discussed in Chapter 4, section 4. The parameter ε is believed to be indicative of deviations from the assumption of simple brownian rotational diffusion due to relatively slowly fluctuating torques that induce the reorientation, and it can be shown to be related to the lifetime of the fluctuating torques experienced by the probe (cf. Chapter 4, section 4.1). The values of ε range between 3 and 15 in different liquid crystals [5,3,14]; these values of ε are comparable to those found for the same spin probe in several isotropic solvents [15]. Another effect which can cause τ_R^B to be unequal to τ_R^C is anisotropic rotational diffusion (i.e., $D_R^{\parallel} \neq D_R^{\perp}$). However, this alternative explanation conflicts with the observations of Hwang et al. [15] that the motion of perdeuteriated tempone-d_{16} is virtually isotropic in a variety of isotropic solvents (and which is also expected on the basis of the geometry of the probe). Therefore, for example, we favor an ε of 10 and isotropic

Table 3. Activation energies and pre-exponential factors for rotational relaxation of perdeuteriated tempone-d_{16} in some liquid crystal (and related) solvents. From [3, 5 and 14].

Phase	Solvent	ln(*A*/*s*)	E_a/kJ mol^{-1}
I	4O.6	-36.1	33.9
I	4O.8	-42.3	52.3
I	8CB	-45.3	62.3
I	Phase V	-37.6	33.5
I	6OCB-8OCB	-42.2	52.7
I	n-Decane	-	12-21
I	di-n-butylphthalate	-	35.8
N	4O.6	-36.8	35.1
N	4O.8	-44.5	15.1
N	8CB	-29.3	17.2
N	Phase V	-38.9	40.2
N	Phase IV	-37.7	37.2
N	BOCP	-36.4	39.3
N	MBBA	-39.5	42.7
N	6OCB-8OCB	-33.2	25.9
S_A	4O.6	-29.1	17.6
S_A	4O.8	-30.0	16.7
S_A	8CB	-36.7	35.6
S_A	S2	-40.0	51.9
S_A	6OCB-8OCB	-36.9	36.0
N_R	6OCB-8OCB	-37.8	38.1
S_B	4O.6	-27.9	8.4
S_B	4O.8	-30.8	16.7

Data taken from [3] (4O.6; 4O.8 and 8CB); [5] (Phase V, Phase IV, bocp, MBBA); [12] (S2) and [14] (6OCB/8OCB).

motion for perdeuteriated tempone-d_{16} in 4O.6 over N ($\equiv D_R^{\parallel}/D_R^{\perp}$) = 4.3.

With the development of time domain ESR methods such as 2D-FT-ELDOR and inversion recovery, we can expect to determine $J(\omega_e)$ directly. From the frequency dependence of $J(\omega_e)$ we could estimate the magnitude of ε without changing the temperature. In this way we may achieve the condition $\omega\tau_R \approx 1$ by simply changing the Larmor frequency, thus enabling a distinction to be made between the two mechanisms described here.

4.3.2. *Ordered Phases.* Most of the liquid crystals studied using perdeuteriated tempone-d_{16} can be generally classified into two groups: the nO.m compounds, which are Schiff bases as shown in figure 4, and the nCB (or nOCB) compounds which are 4-n-alkyl (or alkoxy) -4'-cyanobiphenyls. Examples of the former are MBBA (1O.4), 4O.6 and 4O.8 and some examples of the latter include 8CB, the eutectic mixture S2 and the binary mixture 6OCB-8OCB. In terms of structural resemblance, the eutectic mixture Phase V can be said to belong to the former category.

Here we shall describe relaxation studies of perdeuteriated tempone-d_{16} in the nematic and smectic phases of the liquid crystals shown in figure 4. However, rather than discuss each system individually, we shall present a comparative study of nO.m compounds on the one hand versus nCB (or nOCB) on the other. This is useful in that the former generally form monolayer smectic A phases, while the latter exhibit S_A phases of the bilayer type (S_{A_d}).

Nematic Phase

The range over which the order parameter $\langle D_{00}^2 \rangle$ ($\equiv S$) in these systems varies, is from 0.04 near the N-I transition (i.e., 4O.6) to about 0.20 near the end of the N phase (see figure 6). $\langle D_{20}^2 + D_{-20}^2 \rangle$, which represents the extent of asymmetry in the ordering of the x′ versus y′ axis of the probe with respect to the director, varies between 0.01 and 0.05. These low values for the two order parameters are not surprising, given that perdeuteriated tempone-d_{16} is a near spheroidal probe and, therefore, does not have a preferential direction for alignment. The rotational correlation times, which in the nematic phase vary over a considerable range, lie between 20ps and 500ps (see figure 5); however, this wide range is due to the fact that these liquid crystals exhibit nematic phases at different temperatures (i.e., T_{NI} is very different for these systems). At

a.

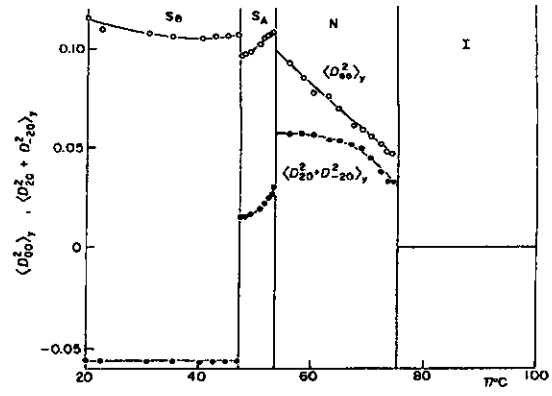

b.

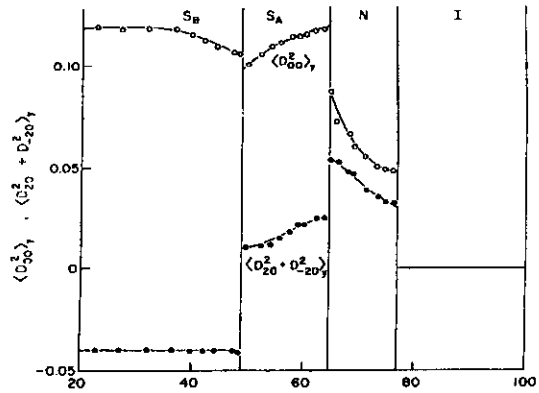
S_B
S_A
N
I
⟨D²₀₀⟩_y
⟨D²₂₀ + D²₋₂₀⟩_y
0.10
0.05
0
-0.05
20
40
60
80
100

c.

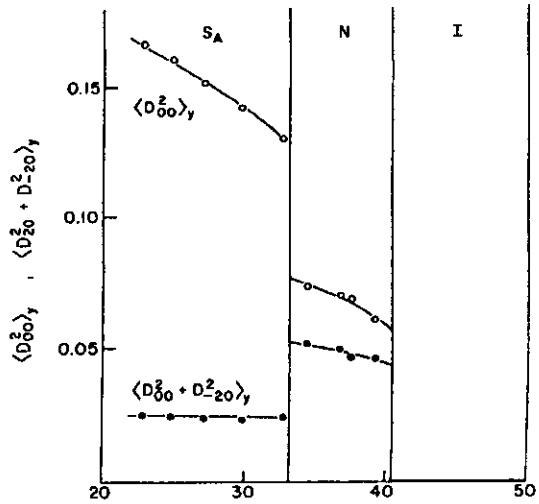
S_A
N
I
⟨D²₀₀⟩_y
⟨D²₂₀ + D²₋₂₀⟩_y
0.15
0.10
0.05
20
30
40
50

d.

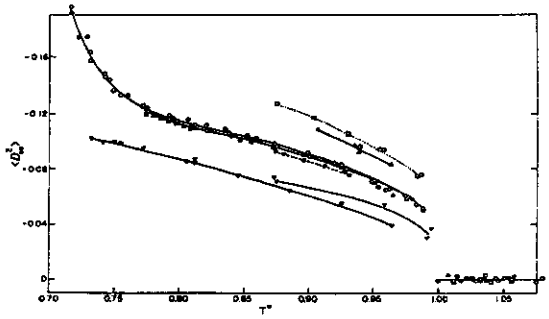

e.

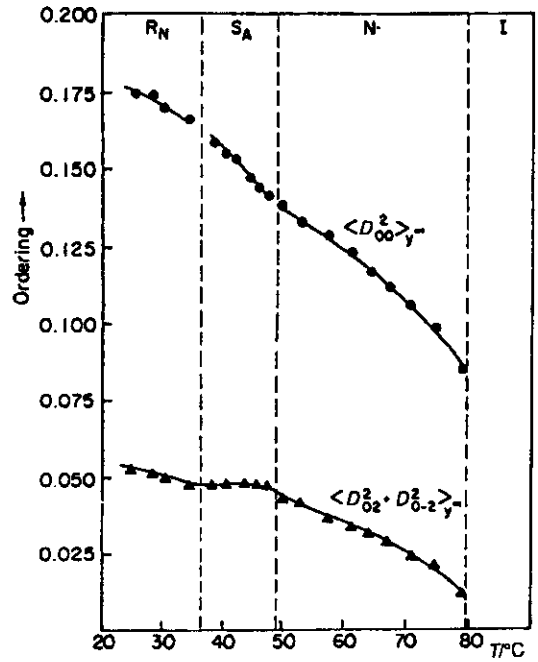

Figure 6. Temperature variation of order parameters $< D^2_{00} >$ and $< D^2_{20} + D^2_{-20} >$ for perdeuteriated tempone in (a) 4O.6; (b) 4O.8; (c) 8CB; (d) Phase-V; and (e) 6OCB-8OCB. The order parameters shown in figure a,b,c, are in error due to faulty measurements of g tensor shifts. The measured hyperfine splittings vary continuously across the second order S_A-N transition. (Sources: a),b),c) [3]; d) [5]. Here $T^* = T/T_{NI}$; Phase V (o); Phase IV (▵); MBBA (o); OHMBBA (▾); BOCP (▿); BECP (▴). e) See [14]).

the high extreme, i.e., τ_R = 500 ps observed in Phase V, the spectra appear to exhibit incipient slow motion. In order to explore this interesting case further, we have recently performed a study of this system at 250 GHz, where the g tensor anisotropy increases by a factor of 30. A comparison of 9 GHz and and 250 GHz spectra appears in figure 7. Such field dependent studies provide a possibility of discerning various motional models (to be discussed later), which in general is difficult to extract just from the fast motional spectra (also see Chapter 15). (Note that the τ_R versus $1/T$ behaviour shown in table 3 for the different systems differs only slightly if we use an axially symmetric potential rather than the correct asymmetric potential. However, the different potentials predict quite different results for the detailed dynamics of asymmetric viscosity about the director. Also, if there is anisotropic rotation about a molecular principal axis, but the molecule is aligned asymmetrically, the use of axial and asymmetric potentials will give quite different results for the ratio of the correlation times, $\tau^{\parallel}_R$ and $\tau^{\perp}_R$. Note that, $\tau_R = \sqrt{\tau^{\parallel}_R \tau^{\perp}_R}$.

An interesting result of our temperature dependent studies in the nematic phase is that whereas for the nO.m compounds the rotational activation energies (E_{act}) are noted to be rather similar in the I and N phases, they are significantly reduced in the N phases (relative to the I phase) of the cyanobiphenyl compounds. Furthermore, the values of E_{act} in the nematic phases of nO.m

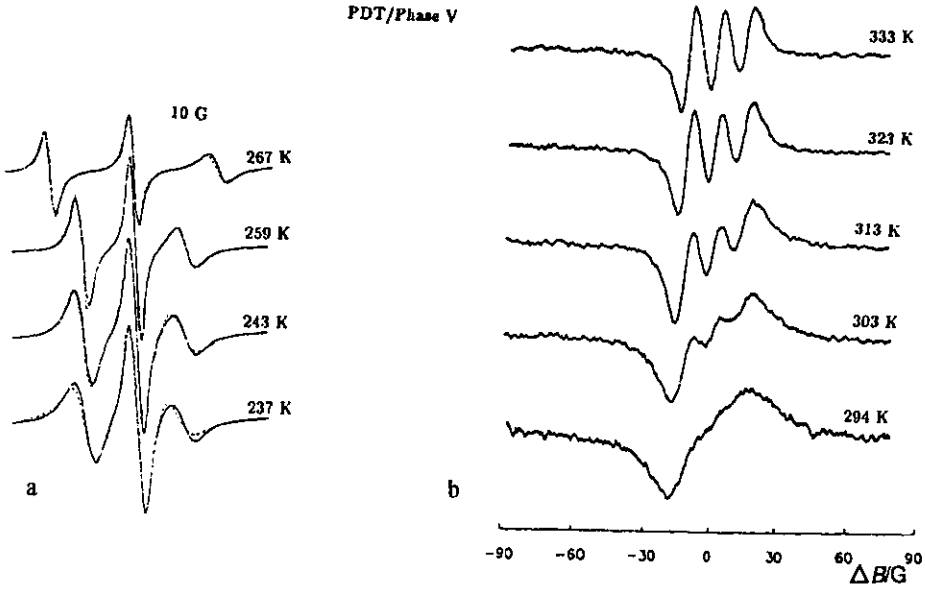

Figure 7. Comparison of spectra from perdeuteriated tempone in Phase V at 9 GHz (a) and 250 GHz (b). [From D. Budil, B. Lynch, K. Earle and J. H. Freed, unpublished results.]

compounds (33-50 kJ mol^{-1}) are similar to E_{act} measured for perdeuteriated tempone-d_{16} in di-n-butylphthalate [10] (37.7 kJ mol^{-1}, cf. table 3), which is an aromatic compound; while, E_{act} in the nematic phases of the cyanobiphenyls (17-25 kJ mol^{-1}) lie closer in magnitude to E_{act} for the probe in alkanes [10] (12-21 kJ mol^{-1}). This observation very strongly suggests that for nO.m compounds perdeuteriated tempone-d_{16} tends to pack with the aromatic cores, but for cyanobiphenyls it resides preferentially among the hydrocarbon chains of the liquid crystal molecules [3,14]. (Further evidence in support of this hypothesis comes from the fact that the isotropic hyperfine coupling constants in the nO.m are more typical of polar solvents, while those for the nCB are comparable to alkanes).

While the ESR spectra fall in the motionally narrowed region in most cases, those for Phase IV and Phase V showed spectra at room temperature with rotational correlation times higher than 100 ps [5]. The results in these cases were first analysed in terms of brownian rotational diffusion in the presence of an orienting potential. It was first assumed that, except for the orienting potential, the description of the motion should be very similar to that for the isotropic liquid, since the values of τ_R do not change very markedly at the phase transition nor is the ordering very substantial (cf. table 3). Thus we used an $\varepsilon \approx 4.6$, which is typical of isotropic liquids. When the best single parameter Maier-Saupe potential was used, it was impossible to fit the results, except with a $\tau_R^B \neq \tau_R^C$. However, with the two parameter potential, τ_R^B and τ_R^C are more nearly equal. The final adjustment (to the results for $\tau_R \leq 10^{-10}$ for $T > 23$°C) was made by fitting ε assuming isotropic rotation under the two term potential. This yielded $\varepsilon = 2.9 \pm 2.4$ (or $\approx 2.2 \pm 1.4$ neglecting one result). However, for $T < 20$°C (or $\tau_R > 2 \times 10^{-10}$) the C/B ratio increases suggesting $\tau_R^B < \tau_R^C$. Very similar behaviour was also observed in a pressure dependent study [16]. The increase in C/B with τ_R is to some extent due to the increase in ordering as either the pressure

is raised or the temperature is lowered. (For an isotropic liquid, *C/B* should remain constant). However, there is a substantial increase in *C/B* with τ_R not attributable to the ordering. This may be interpreted in terms of (i) anisotropic viscosity; (ii) anisotropic diffusion; (iii) modification of the pseudo-secular spectral densities by analogy with the non-secular corrections (cf. table 1) by introducing an ε'. For example, it was found that $\varepsilon' \approx 5$ in the viscous isotropic solvent glycerol. None of these explanations were found to be satisfactory. When the results are analysed in terms of anisotropic viscosity, the value of $\hat{N} \equiv \hat{D}_R^{\parallel}/\hat{D}_R^{\perp}$ continues to increase with decreasing $\hat{D}_R^{\perp}$ (i.e., $\hat{D}_R^{\parallel}$ remains nearly constant while $\hat{D}_R^{\perp}$ decreases considerably). When the results are analysed in terms of anisotropic diffusion, we find that $N_y = D_R^{\parallel}/D_R^{\perp}$ must be increasing as $D_R^{\perp}$ decreases, and this is turned on only for $\tau_\perp \equiv (6D_R^{\perp})^{-1} > 200$ ps. Furthermore, when $\tau_R \geq 1$ ns, A' is predicted to be negative from such an analysis, which is physically impossible; typically A' increases with increasing τ_R in the range $\tau_R \geq 100$ ps (cf. [15]). The modification of the pseudo-secular spectral density with $\varepsilon_{\text{pseudosecular}}$, i.e., $\varepsilon' \approx$ 13-20 yields results for τ_R equal to that of the values of $\hat{\tau}_\perp \equiv (6\hat{D}_R^{\perp})^{-1}$ for the anisotropic viscosity model. However, a single, and constant, parameter (ε') adequately explains a range of results. Thus the analysis in terms of ε' is a useful way of representing the data, but questions remain as to the validity of using such a large ε' [5], and so the SRLS model is somewhat favoured.

In general, we note that in the motionally narrowed region, it is difficult to discern between models of rotational dynamics such as (i) anisotropic brownian motion, (ii) anisotropic viscosity, (iii) fluctuating torques, and (iv) SRLS, without additional considerations. However, in the cases where slow motional spectra are observed, the use of non-Debye spectral densities (i.e., ε') is found to improve significantly the simulations to the experimental spectra. This indicates that brownian diffusion in the presence of an orienting potential provides an oversimplified description of the dynamics, which in this case is better modeled in terms of fluctuating torques or SRLS (cf. Chapter 4, section 4).

Smectic A Phase

The liquid crystals shown in figure 2 exhibit second order S_A-N phase transitions, with the exception of S2 which exhibits a weakly first order transition. Accordingly, the order parameter *S* for perdeuteriated tempone-d_{16} changes smoothly upon cooling from the N into the S_A phase [17,18,12,14]. A more detailed discussion of the ordering at the vicinity of the S_A-N transition appears in Chapter 13, sections 1 and 2.

From a spin relaxation viewpoint, there are two fundamental properties of smectic phases that distinguish them from nematic phases.

(i) It is possible to lock the S_A director in a chosen orientation relative to the static magnetic field [3,19], thereby permitting angle dependent studies to be performed. Thus, more detailed dynamic information can be obtained than by performing studies at a fixed orientation. (Note however, that angle dependent electron spin relaxation studies have also been performed in a nematic liquid crystal using electric fields to lock the director [11].)

(ii) The layered structural arrangement of the S_A phase causes the rotational diffusion of a solute (i.e., the probe molecule) to be influenced by its translational behaviour. That is, as the molecule translates in directions normal to the layers, it experiences changes in the orienting potential (cf. Chapter 3, section 2.5 and Chapter 4) which thus causes its rotational motion to be modulated. Therefore, a proper treatment of relaxation in smectic phases must include the finite effects of roto-translational coupling [20,12].

As expected for a more viscous phase, the rotational corelation times for perdeuteriated

tempone-d_{16} in the S_A phase are somewhat higher than in the N phase for a given liquid crystal (see figures 5a-5e). They lie between 50 (50-60 ps for 4O.8) to 500 ps (170-500 ps for 8CB). However, the increases in τ_R in the S_A phase are accompanied by a decrease in E_{act} for the nO.m compounds [3,14]. This observation supports the view that the perdeuteriated tempone-d_{16} is expelled more into the hydrocarbon regions of the smectic layers due to the smectic packing (as compared to the nematic phase, in which polar interactions of the nitroxide group with the central portions of nO.m compounds are favoured). The case with cyanobiphenyls, where E_{act} in the S_A phase is higher than in N, can be interpreted on the basis of the hypothesis that in the nematic phase, the perdeuteriated tempone-d_{16} is already expelled into the hydrocarbon regions due to association of cyano groups but in the smectic phase, in which interdigitated bilayers form, the aliphatic region is bounded by better defined layers of cyano groups to which the probes can make more contact (see also re-entrant nematic phase, later).

The τ_R results for 4O.6, 4O.8 and 8CB were explained most satisfactorily in terms of SRLS, as the temperature in the S_A phase decreases, the order parameter S_1 for the SRLS increases as S_1^2 [3,21]. In our past work [3] we had considered an isotropic SRLS model in the smectic phases of these liquid crystals. We shall present our most recent work on smectics shortly, but before that we digress to note some of the experimental difficulties we encountered in the study of smectics.

A comparison of orientation dependent spin-echo and estimates of CW homogeneous linewidths (obtained by the deconvolution of deuteron superhyperfine structure) in the smectic phase of S2 reveals that the CW linewidths are consistently larger than the pulsed linewidths, implying an additional source of inhomogeneous line broadening. We have studied this effect as a function of (a) sample geometry (such as plate versus capillary samples of varying size), and found that this effect is a result of complex wall anchoring effects which tend to propagate over macroscopic distances from the wall of the container, and (b) the magnetic field effect associated with the anisotropic susceptibilty of liquid crystals. The latter tends to align the smectic layer normal parallel to the external field, however this tendency is opposed by the smectic elastic coefficients transmitting the effects of wall anchoring. Thus, an equilibrium distribution of the directors is rather complex, and depends upon the boundary conditions and the factors discussed here. Experimentally, the effect is assessed by measuring the asymmetry of the hyperfine lines. In our experience, the plate geometry provides the best conditions for aligning ESR samples homogeneously, but the degassing procedure to eliminate oxygen broadening becomes more tedious and perdeuteriated tempone-d_{16} tends to plate out on the walls [3,11]. To overcome this difficulty we have tried to simulate orientation dependent spectra invoking a director distribution that changes when the director orientation is changed with respect to the external applied magnetic field. Even in the capillary samples the orientational distribution is strongly peaked about the mean director, but the errors in the actual homogeneous linewidths could be as high as 20-30%. We show in figure 8 a comparison of homogeneous linewidths as determined by CW and pulsed techniques in the smectic phase of the S_2 liquid crystal. This is for 0° rotation for which these problems are actually minimised. Note that the most significant deviations occur for the $M_I = +1$ hyperfine line, which is due to the fact that for this line $\Delta P/w$ where ΔP is the difference between the resonant position at the 0° and 90° orientation of the director (with respect to B_0) and w is the average width, is the largest. This feature affects the calculation of B most significantly (cf. equation (32)).

The T_2 obtained from the spin-echo methods are more reliable, because they can be obtained without deconvoluting the lineshapes and they are indepedent of inhomogeneous linewidths [22]. In addition, new time domain two dimensional Fourier transform techniques make it possible to determine W_n and W_e. The combination of these techniques and orientation dependent studies

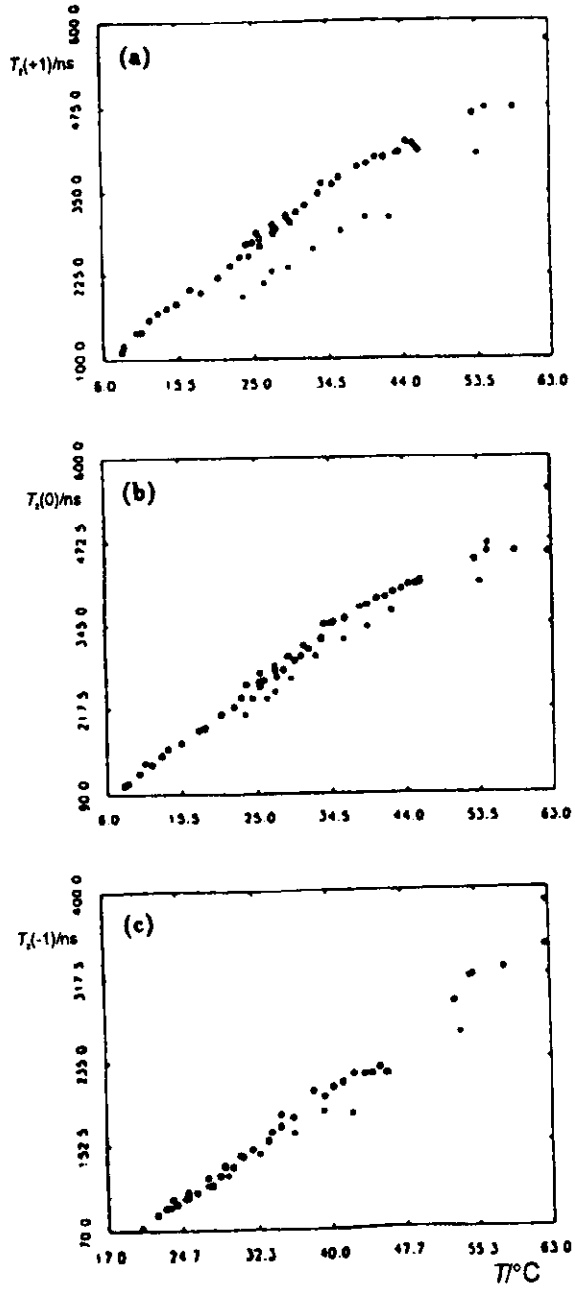

Figure 8. Comparison of T_2's, i.e., homogeneous linewidths, as obtained from CW (●) and ESE (○) methods for perdeuteriated tempone in S2: (a) low field line (b) middle field line and (c) high field line. (From [12]).

enables us to determine individual spectral densities, $J_i(0)$, $J_i(\omega_n)$ [12] which allows a more careful analysis of spin relaxation data for perdeuteriated tempone-d_{16} in the smectic phase of S2. The two salient features of the data are, the nearly orientation independence of B and C and the strong orientation dependence of W_n as shown in figure 6. We first discuss the former and then the latter in order to assess the ability of the motional models to explain our results.

(i) W_n, **Nuclear Spin Relaxation**: We found, in general $J_1 < J_0$, J_2 which rules out (1) the ODF (orientational fluctuations of the director) model since ODF is expected to enhance J_1; (see Chapters 9 and 14 for a detailed discusssion of the ODF mechanism) (2) anisotropic brownian motion predicts $J_0 > J_1 > J_2$ and so this model also fails to predict the observed variation of W_n (or in fact its order of magnitude); (3) a combination of anisotropic viscosity and anisotropic brownian motion was also unsuccessful.

A model wherein we take into account the roto-translational coupling, proposed by Moro and Nordio based on a general rotational-translational Smoluchowski formalism discussed by Hwang and Freed [23,5], is able to account for our results. In this model, the McMillan potential (cf. Chapter 4, section 2.5) is used. Physically, it represents the fact that as the probe molecule diffuses in the direction normal to the smectic layers it experiences a variable orienting potential that depends on its location in the layer, its magnitude being largest at the cores and smallest in the tails of the alkyl groups. In addition, the translational diffusion rates must be sufficiently slow compared to the τ_R such that, on the ESR time scale the probe experiences fluctuations in the orientational potential and not just a mean orientational potential. It is in this respect that the model falls under the general class of SRLS models discussed in Chapter 4.

Table 4. Parameters obtained from orientation-dependent W_N simulations with the Moro-Nordio model of solute dynamics in smectics. (From [12])[a].

T/°C	A	B	C	τ_R/ps	D_T^{zz}/cm^2 s^{-1} [b]	S	S_{MAX}	σ	γ
15.45	-3.40	-2.73	2.205	131.5	1.14 x 10^{-6}	0.453	0.823	0.042	0.294
20.25	-3.20	-2.60	2.073	143.4	1.41 x 10^{-6}	0.434	0.812	0.048	0.294
26.15	-2.60	-2.55	1.820	130.4	3.42 x 10^{-6}	0.337	0.785	0.105	0.294
30.95	-2.27	-2.40	1.630	76.0	3.08 x 10^{-6}	0.294	0.759	0.119	0.294
37.86	-1.70	-2.57	1.426	67.8	5.47 x 10^{-6}	0.185	0.732	0.184	0.294
42.60	-1.52	-2.39	1.299	59.2	> 25 x 10^{-6}	0.167	0.704	0.177	0.294

[a] The coefficients A, B and C are implicitly defined in Chapter 4, equation (31). Also $S = \langle P_2(\cos\beta)\rangle$, $\sigma = \langle\cos(2\pi z/d)\, P_2(\cos\beta)\rangle$ and $\gamma = \langle\cos(2\pi z/d)\rangle$.

[b] Obtained with a bilayer thickness d = 3.0 x 10^{-7}cm.

Our results are summarised in table 4. The important parameters that are needed are the potential terms (cf. equation (31) of Chapter 4) A, B, C and translational (D_T^{zz}) and rotational diffusion coefficients $D_R^{\perp}/D_R^{\parallel}$. This is a total of six parameters! Unfortunately, with only four parameters J_1, J_0, J_2, $A + B$ (the last parameter is the ordering potential at the cores which is estimated from the CSL ordering, see Chapter 15), it is essential to make certain approximations. We chose to fix $\gamma \equiv \langle\cos 2\pi z/d\rangle$, which is reasonable for results collected for

($| T - T_{S_AN} | > 3°C$) from the smectic A-nematic transition. Also we let $N = 0.8$. We find that τ_R and D_T^{zz} are not uniquely determined at a given temperature, but they can be better determined by considering the entire temperature dependent data set. We note here that D_T^{zz} is not the macroscopic translational diffusion coeffcient, but it represents a diffusion coefficient determined on the short time scale (of the 2D-FT-ELDOR experiment ≈ 300-800 ns) or equivalently the microscopic diffusion coefficient, and it should be compared with the techniques that measure the diffusion coefficients on a microscopic scale such as the Heisenberg spin exchange method. Indeed, the recent measurements [44] of the macroscopic translational coefficient ($D_T^{\parallel}$) of perdeuteriated tempone-d_{16} in S2 are about an order of magnitude slower than the other values reported in table 5, while the diffusion coefficients of perdeuteriated tempone-d_{16}, determined from the Heisenberg spin exchange technique in similar liquid crystals 6OCB-8OCB (cf. table 6) are comparable to the diffusion coefficients obtained from our analysis.

Table 5. Macroscopic translational diffusion constants measured by DID-ESR. (From [43,44]).

Host Material	Probe	T/K	D_T/cm^2 s^{-1}
H_2O	TEMPONE[a]	295	1.7×10^{-5}
C_2H_5OH	2,5DTBSQ[b]	295	2.7×10^{-5}
5,4[A] (iso)	TEMPONE	323	2.5×10^{-6}
5,4 (nem) $D_T^{\perp}$	TEMPONE	300	9.0×10^{-7}
5,4 (nem) $D_T^{\parallel}$	TEMPONE	300	6.4×10^{-7}
MBBA[B] (nem) $D_T^{\perp}$	^{15}N - PDT[c]	293	2.5×10^{-7}
MBBA (nem) $D_T^{\parallel}$	^{15}N - PDT	293	3.7×10^{-7}
Phase V[C] (nem) $D_T^{\perp}$	TEMPONE	294	1.25×10^{-7}
Phase V (nem) $D_T^{\perp}$	OBSL[d]	294	0.48×10^{-7}
S2[D] (smectic) $D_T^{\parallel}$	TEMPONE	294	0.95×10^{-7}
S2 (smectic) $D_T^{\perp}$	TEMPONE	294	2.0×10^{-7}
S2 (smectic) $D_T^{\parallel}$	CSL[e]	294	7.94×10^{-8}
S2 (smectic) $D_T^{\perp}$	CSL	294	5.75×10^{-8}

[A] 4-n-pentylbenzylidene-4'-n-butylaniline
[B] 4-methoxybenzylidene-4'-n-butylaniline
[C] nematic mixture
[D] smectic mixture

[a] 2,2,6,6,-tetramethylpiperidrine-l-oxyl
[b] 2,5-di-t-butyl-para-benzosemiquinone
[c] perdeuteriated tempone-d_{16} (^{15}N-labelled)
[d] octylbenzoyl spin label
[e] 4,4-dimethylspiro oxazolidine-2,3'-5α cholestane-3-oxy.

Table 6. Microscopic translational diffusion rates as measured by HE for perdeuteriated tempone-d_{16} in 4O.6 and 6OCB-8OCB. (From [25])

Table 6a. Non-linear least square analysis of fits to $k = A\exp(-\Delta E_{act}/RT) + B\exp(\Delta E_{act}/RT)$.

System	Phase	A/G M^{-1}	B/G M^{-1}	ΔE_{act}/kJ mol^{-1}
PDT/4O.6	I	$(1.9 \pm 0.1) \times 10^{6}$	$(9.7 \pm 0.6) \times 10^{-5}$	33.7 ± 0.3
	N	$(5.3 \pm 0.5) \times 10^{3}$	$(3.5 \pm 0.3) \times 10^{-2}$	15.5 ± 0.3
	S_B	$(6.8 \pm 1.2) \times 10^{5}$	$(1.6 \pm 0.3) \times 10^{-4}$	27.4 ± 0.5
PDT/6OCB-8OCB	I	$(1.9 \pm 0.1) \times 10^{4}$	$(1.7 \pm 0.1) \times 10^{-2}$	18.5 ± 0.2
	N, S_A, N_R	$(9.5 \pm 3.0) \times 10^{3}$	$(1.4 \pm 0.4) \times 10^{-2}$	16.0 ± 0.9

Table 6b. Dipolar Contributions and Diffusion Coefficients.

System	Phase	T/°C	T_2^{-1}(HE)/T_2^{-1}(dip)	$D_T \times 10^6$/cm^2 s^{-1} [a]
PDT/4O.6	I	85	3.30	1.16
	N	70	3.14	1.14
	S_B	40	3.39	0.91
PDT/6OCB-8OCB	I	85	4.88	1.87
	N	60	7.10	1.45
	S_A	40	3.42	1.01
	N_R	28	2.10	0.79

[a] Calculated from the HE contribution ($A\exp(-E/RT)$), and assuming $d = 6.4$ Å for perdeuteriated tempone-d_{16}.

(ii) **Orientation independence of *B* and *C*.** One of the main outstanding problems in this study is the virtual orientation independence of the B and C terms. All of the models we have attempted to use lead to a significant orientation dependence. We have been unsuccessful in fitting simultaneously orientation dependent W_n and orientation independent B and C data. One hint comes from fact that the $J(0)$ which affect B and C are significantly larger than the $J(\omega_a)$. This suggests an additional relaxation mechanism that affects selectively $J(0)$ or near zero frequency spectral densities over the $J(\omega_a)$, or frequencies greater than 10^6 s^{-1}. Since the McMillan form of the potential favours probe expulsion in the alkyl chains, we may conjecture an isotropic SRLS model where the alkyl chain matrix surrounding the probe provides low frequency motional modes that affect $J(0)$ but not $J(\omega)$ [12]. Note that our results from table 6 imply that $< D_{00}^2 >$ is virtually zero in the alkyl chains.

Reentrant Nematic Phase

With a view to discerning possible differences in the dynamic molecular structures between

normal nematic (N) and reentrant nematic (N_R) phases (i.e., when the nematic phase reenters upon cooling from the smectic phase [24]), we have also studied a liquid crystal exhibiting a reentrant nematic phase, 6OCB-8OCB. Our studies with perdeuteriated tempone-d_{16} in 27wt.% 6OCB in 8OCB showed that (i) the ordering in the N_R phase was higher than that in the N and S_A phases, but with no abrupt changes in the ordering occuring as a function of temperature, and (ii) while the rotational correlation times in the N_R phase are slightly higher than in the S_A phase, the activation energies are comparable in the two phases (and are higher than in the N phase).

Our results further show (see also our studies in 6OCB-8OCB with spin probes other than perdeuteriated tempone-d_{16} in Chapter 15, section 3, and [14]) that as smectic layers begin to form, the probe molecules are expelled from the aromatic core regions to the aliphatic chains. However, the somewhat increased activation energy in the S_A phase (36.0 kJ mol^{-1}) relative to the N phase (25.9 kJ mol^{-1}) is behaviour similar to that observed for perdeuteriated tempone-d_{16} in 8CB [3] (see table 3 and figure 5e). This suggests a little more access to the aromatic core region once ordered smectic layers form [14]. As the temperature is lowered even further, the reentrant nematic phase is formed with very little change in the rotational dynamics of perdeuteriated tempone-d_{16}. Given that the activation energies in the S_A and N_R phases are comparable, and that the ordering changes continuously across the S_A-N transition, the results imply that the structural changes which the liquid crystal undergoes at the N_R - S_A transition are very subtle, with nothing dramatic occuring. Furthermore, at least from a microscopic point of view, there are essentially no discernible differences between the S_A-N transition in normal compounds (i.e., 8CB) and those that exhibit reentrant nematic behaviour. (Note that apart from 8CB and 6OCB-8OCB being structurally similar types of molecules (they are both cyanobiphenyls), they both form bilayer S_A phases.)

5. Translational Motion in Liquid Crystals

In the study of molecular dynamics in condensed media by ESR, there is need for a convenient technique for measuring translational diffusion coefficients, D_T, for the spin probes. Experiments designed to measure D_T can be divided into two general categories: microscopic and macroscopic. A typical microscopic method used in ESR is the measurement of Heisenberg spin exchange (HE) between colliding radical pairs. Line broadening due to such a method measures diffusion over dimensions on the order of molecular lengths [6,25]. The analysis leading to the diffusion coefficient depends upon the choice of the molecular model, a feature that is characteristic of microscopic methods in general. On the other hand, macroscopic methods, such as NMR field-gradient spin-echoes, involve diffusion over macroscopic distances. These experiments may be interpreted in terms of the simple phenomenological description of diffusion to yield D_T [33]. A combination of microscopic and macroscopic measurements can be employed to understand better the details of molecular motions important for diffusion at all scales of distance.

In this section, we describe the two approaches that have been used in our laboratory for studying translational motion using nitroxides in some liquid crystals: HE, and dynamic imaging of diffusion by ESR (DID-ESR).

5.1. MICROSCOPICS: HEISENBERG SPIN EXCHANGE

The phenomenon of Heisenberg spin exchange, in which two radicals collide, and which effectively results in the electron spins S_1 and S_2 exchanging their nuclear environments, is a time dependent and diffusion controlled process resulting from the relative motion of radical pairs [27].

During the (bimolecular) collision, the exchange interaction that occurs is described in terms of the hamiltonian H_{ex}:

$$H_{ex} = J(t)\,\mathbf{S}_1.\mathbf{S}_2, \tag{51}$$

where $J(t)$ is twice the (time-dependent) exchange integral. The time dependence of J is taken into account implicitly through the dependence of J on $\mathbf{r}$ and Ω, which specify the distance and orientation of a given radical with respect to another.

A quantity of fundamental interest in HE studies is ω_{HE}, the spin exchange frequency; this is directly proportional to the concentration of spins in the system. When the solutions are not too concentrated (concentrations below 15 mM in typical fluids), the slow exchange condition, characterised by $\omega_{HE} \ll \gamma_e a_N$ for nitroxide spin probes, obtains. Under these conditions, and assuming a contact exchange model (i.e., that exchange occurs for every bimolecular collision regardless of the relative orientation of the radicals), it has been shown that under strong exchange conditions (see later) [28]:

$$\omega_{HE} = \tau_2^{-1} = (\sqrt{3}/2)\, f_M\, \gamma_e \left[\delta_M - \delta_M(0)\right], \tag{52}$$

where τ_2 is the mean time between successive bimolecular collisions; δ_M and $\delta_M(0)$ are the first derivative ESR intrinsic linewidths of the line of spectral index M in the presence and absence of exchange, respectively. The subtraction effectively eliminates all contributions to spin relaxation that are independent of concentration, leaving only intermolecular mechanisms. In equation (52), M refers to a given hyperfine line in the spectrum (for ESR spectra from ^{14}N-nitroxides $M = 1,0,-1$ correspond to the low, central and high field lines, respectively), and f_M is a statistical factor related to the degeneracy (and thus intensity) of the ESR transition(s) describing that line:

$$f_M = N/(N - 2D_M), \qquad N = \sum_M D_M \tag{53}$$

Here, N is the total number of spin eigenstates, and D_M denotes the degeneracy of the Mth eigenstate where M refers to the nuclear spin quantum number identifying the eigenstate(s) involved in the particular ESR transition. For nitroxide radicals (neglecting proton or deuterium superhyperfine splitting), $N = 6$ ($I = 1$, $S = 1/2$), and since the eigenstates are non-degenerate, $D_M = 1$; thus $f_M = 3/2$.

For brownian diffusion involving neutral radicals, τ_2 is related to the radical diffusion constant D_T by [28]:

$$\tau_2^{-1} = 4\pi d\, D_T \rho, \tag{54}$$

where d is the encounter distance for two radicals undergoing exchange, D_T is the translational diffusion coefficient for the self-diffusion of the radicals, and ρ is the number density of radicals [28,33]; (ρ is related to the molar concentration C of the solution by $\rho = 10^{-3} N_A C$). Equations (52) and (54) show that, for strong exchange, $d\omega_{HE}/dC$, the slope of the variation of ω_{HE} with spin concentration is directly proportional to D_T. For translational diffusion in isotropic liquids, the Stokes-Einstein relationship gives for self-diffusion

$$D_T = k_B T/6\pi r\eta, \tag{55}$$

where r is the hydrodynamic radius of the diffusing molecule (in HE studies, the spin probe), and η is the absolute viscosity. We shall assume that $r = d/2$. For diffusion in liquid crystals, it has

been suggested that D_T may be visualised as a mean of the diffusion constants $D_T^{\parallel}$ and $D_T^{\perp}$ (i.e., $D_T = (D_T^{\parallel} + 2D_T^{\perp})/3$), and η may be replaced by an effective viscosity, defined as a mean of the viscosities in directions parallel and perpendicular to the magnetic field [29]. It will also be noted that for a Stokes-Einstein hydrodynamic model,

$$D_T^{r} = 2k_B T/3\pi d\eta \tag{56}$$

for the relative diffusion of the radicals.

Equation (52) corresponds to the strong exchange limit, i.e., the situation which obtains when the radical pair is sufficiently long lived that the condition $J_0^2 \tau_1^2 \gg 1$ is fulfilled; here τ_1 is the mean lifetime of a radical pair and J_0 is the contact value of $J(r)$. More generally, however, [30]:

$$\omega_{HE} = \tau_2^{-1}\left[J_0^2 \tau_1^2/(1 + J_0^2 \tau_1^2)\right]. \tag{57}$$

Here τ_2 is related to D_T via equation (54), whereas τ_1 is related to D_T by:

$$\tau_1^c = d^2/6D_T \tag{58}$$

for a contact exchange model [31], or

$$\tau_1(\lambda) \approx d^2(1 + \lambda d)/2D_T \lambda^2 d^2 \tag{59}$$

for a model that allows for the finite range of the exchange interaction, i.e., [32]

$$J(r) = J_0 \exp\left[-\lambda(r - d)\right].$$

Thus λ specifies the range of the exchange interaction, and d is the distance of closest approach of the radicals. Equations (59) and (58) can be generalised to include the effect of interaction potentials between radicals and of the liquid structure via a pair correlation function as discussed later. From equations (54), (57), (58) and (59), we note that as the mechanism of spin exchange changes from strong to weak, the power law dependence of ω_{HE} on D_T changes from 1 to -1. Therefore, the quantity obtained by measuring the slope of the excess linewidth versus concentration (at a given temperature) will be linearly proportional to D_T only in the limit of strong exchange, a consideration that is useful in the context of our experiments with the more anisotropic P-probe.

When the two interacting radicals display anisotropic features in their spin exchange, only those collisions for which the colliding radicals are favourably oriented will lead to spin exchange. The measured exchange rate could, therefore, appear smaller than that calculated on the basis of an isotropic exchange model. In this case, the exchange interaction can be described in terms of an orientation dependent exchange integral $J(r, \Omega_1 \Omega_2)$, where r is the inter-radical separation, and Ω_1 and Ω_2 are Euler angles specifying the orientation of each of the two radicals in the laboratory fixed frame [34]. When one of the radicals involved is spherically symmetric while the other is axially symmetric about some molecular axis, then Zientara and Freed [34] showed that $J = J(r,\theta)$, and they suggested the form:

$$J(r,\theta) \approx \left[J_0 + (J_1/2)(1 + \cos\theta)\right]\exp\left[-\lambda(r - d)\right], \tag{60}$$

with θ being the angle between the inter-radical axis and the symmetry axis of the non-spherical radical. In the limit when the anisotropies are averaged out due to rapid rotation of the radicals (see later), this equation becomes:

$$J(r) = \left[J_0 + (J_1/2)\right]\exp\left[-\lambda(r-d)\right]. \tag{61}$$

The result in equation (60) may be generalised to the case of two interacting non-spherical radicals [34]. In this case, we may write $J = J(r,\theta'_1,\theta'_2,\phi'_1-\phi'_2)$, where θ'_i,ϕ'_i denote the polar and azimuthal angles that the p orbital centered on radical i (= 1 or 2) has in a cartesian coordinate system where the inter-radical axis is the z axis. A generalisation of equation (60) to this case might be:

$$J(r,\theta'_1,\theta'_2,\phi'_1-\phi'_2) = J_\sigma \cos\theta'_1 \cos\theta'_2\left[\cos\theta'_1\cos\theta'_2 + \sin\theta'_1\sin\theta'_2\cos(\phi'_1-\phi'_2)\right], \tag{62}$$

where J_σ denotes the magnitude of the exchange integral when the two p orbitals on the nitroxide radicals overlap along the inter-radical axis, and is assumed to contain the r dependence (of the same form as in equation (60)). The polar coordinates of the inter-radical axis in the laboratory frame are β and γ, whereas those for the symmetry axes of the ith radical are β_i^0 and γ_i^0.

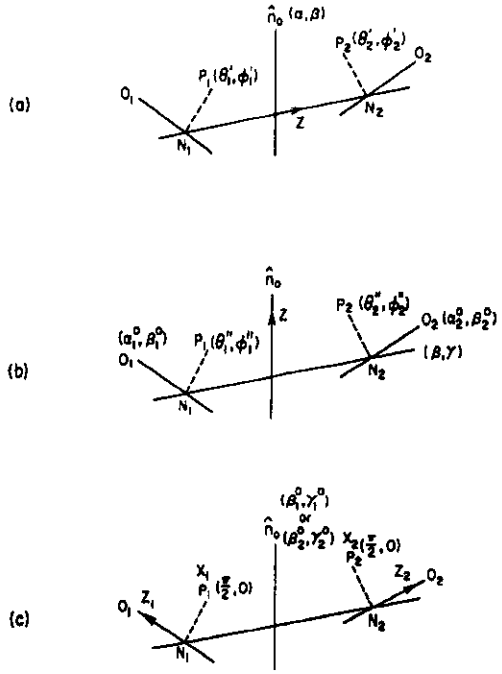

Figure 9. Relative orientations of two nitroxide radicals N_1O_1 and N_2O_2 in different cartesian coordinate systems as discussed in the text. The p orbitals lie along N_1-P_1 and N_2-P_2. In each case, the z axis of the coordinate system is indicated by an arrow, and the polar coordinates of the relevant vectors are shown in that coordinate frame. (a) The internuclear system; (b) the laboratory system; (c) the molecular systems. (From [25]).

The different coordinate systems discussed here are shown in figure 9. Thus, if θ_i denotes the polar angle that the symmetry axis of radical i makes with the internuclear axis, then

$$\cos\theta_i = \cos\beta_i^0 \cos\beta + \sin\beta_i^0 \sin\beta \cos(\gamma_i^0 - \gamma). \tag{63}$$

The effect on the magnitude of J of rotation of the spin probes along their symmetry axes is discussed in detail later. The important point in these cases is that the molecular orientations are referred to the inter-radical axis.

When the rotational correlation time of the radical, τ_R, is shorter than τ_1, the anisotropies may be averaged out during the exchange encounter [34]. Note that in a Stokes-Einstein model,

$$\tau_R = \kappa\tau^*/6, \tag{64}$$

with $\tau^* \equiv \pi\eta d^3/k_BT$, and where the factor $\kappa \leq 1$ allows for rotational slip of the radicals. In this notation, equations (58) and (59) (with equation (56)) become:

$$\tau_1(\lambda) = (3/2)\tau^*(\lambda d)^{-2}(\lambda d + 1),$$

and

$$\tau_1^c = \tau^*/4 = (3/2)\tau_R/\kappa.$$

Thus, smaller values of κ (i.e., < 1) would lead to the anisotropies of J in equations (60) and (62) being averaged out.

In liquid-crystalline phases, the distribution function for the orientation of the ith type of molecule, $P(\Omega_i^0)$, is no longer uniform. In general, it is axially symmetric about the preferred direction of alignment, i.e., the director (for a uniaxial liquid crystal). For an axially symmetric molecule, $P(\Omega_i) = P(\beta_i^0)$. However, even though $P(\beta_i^0)$ may be non-uniform, it is quite possible for $P(\beta)$, the distribution function for the orientation of the inter-radical axis, to be uniform. (We would expect this to be the case for nematic phases.) In that case, the average of $\cos\theta_i^0$ over the distribution, $P(\beta)$, is seen to be zero, showing that there is no preferential value of the θ_i^0 when the radicals collide. However, it also follows from equation (63), that given some initial value of β at the outset of a molecular collision, the non-uniform $P(\beta_i^0)$ will imply incomplete rotational averaging of the $\cos\theta_i^0$. Thus, the effective J in a collision will become a function of β, and some collisions will have the characteristics of strong exchange, whereas for others it would be weak exchange, provided J is strongly anisotropic. In what follows we shall sketch the effect of ordering on J. For the purpose of simplicity we shall consider only the case where spin labels are axially symmetric and the orientational potential contains only the λ_{20} term. Nevertheless, the final form can easily be generalised to contain higher terms in the potential, as required, when we are dealing with liquid-crystalline phases of lower symmetry.

5.1.1. *Anisotropic effects in spin exchange.* We start with the expression for J given by equation (62). As shown in figure 9, for nitroxides the z axis lies along the inter-radical axis connecting the nitrogen atoms N_1 and N_2 of the two nitroxide radicals N_1-O_1 and N_2-O_2. For simplicity, each N-O bond is assumed to lie along the symmetry axis of the molecule containing the bond. The (θ'_i, ϕ'_i) are the polar coordinates of the p orbitals N_i-P_i centered on N_i. (Note that N_i-O_i is perpendicular to N_i-P_i.)

We now consider the effect upon J of (rapid) rotations about the axes N_i-$O_i(\theta_i,\phi_i)$ i.e., the molecular symmetry axes. The effect of rotational transformations on J is simplified on expressing

the latter in terms of spherical harmonics according to:

$$J = (4\pi/3) J_0 (A/3 - B/5), \tag{65}$$

where

$$A = (4/5)\, Y_{2,0}(\theta'_1 \phi'_1)\, Y_{2,0}(\theta'_2 \phi'_2) + (1/\sqrt{5\pi})\left[Y_{2,0}(\theta'_1 \phi'_1) + Y_{2,0}(\theta'_2 \phi'_2)\right] + (1/4\pi) \tag{66}$$

and

$$B = Y_{2,1}(\theta'_1 \phi'_1)\, Y_{2,-1}(\theta'_2 \phi'_2) + Y_{2,-1}(\theta'_1 \phi'_1)\, Y_{2,1}(\theta'_2 \phi'_2). \tag{67}$$

(Note that equation (62) was chosen in part to allow this simple decomposition into spherical harmonics).

We shall now express J in a laboratory fixed frame, so that the anisotropy of J can be expressed in terms of variables that describe the ordering of the probe molecules. This transformation is achieved in two steps: (i) a transformation from the internuclear frame (abbreviated as int), defined such that its z axis lies along the internuclear axis N_1-N_2 and its x axis lies in the plane containing the N_1-O_1 bond, to the laboratory frame (lab) defined such that its z axis lies parallel to the mean director. The Euler angles for this transformation are ($\alpha\beta\gamma$). (ii) A transformation from the laboratory frame to the molecular frame (mol), defined as having its z axis along the N_i-O_i bond, and its x axis along the p orbital N_i-P_i. The appropriate Euler angles are $(a_i^0, \beta_i^0, \gamma_i^0)$. With these definitions, we have [7]:

$$\begin{aligned} Y^{\text{int}}_{2,m}(\theta'_i \phi'_i) &= \sum_{m'} Y^{\text{lab}}_{2,m'}(\theta''_i \phi''_i)\, D^2_{m',m}(a,\beta,\gamma)_{\text{lab}\to\text{int}} \\ &= \sum_{m'} \sum_{m''} Y^{\text{mol}}_{2,m''}(\theta_i^m \phi_i^m)\, D^2_{m'',m'}(a_i^0\, \beta_i^0\, \gamma_i^0)_{\text{mol}\to\text{lab}}\, D^2_{m',m}(a\beta\gamma)_{(\text{lab}\to\text{int})}. \end{aligned} \tag{68}$$

In these equations, $(\theta''_i \phi''_i)$ and $(\theta_i^m \phi_i^m)$ are the polar coordinates of the orbital N_i-P_i in the laboratory and molecular frames, respectively. Note that since in the latter frame, the x_i axes are chosen to lie along the N_i-P_i direction, it follows that $(\theta_i^m \phi_i^m) \equiv (\pi/2, 0)$. Also, $(\beta\gamma)$ denote the polar coordinates of the internuclear vector in the director (i.e., laboratory) frame, and $(a_i^0\, \beta_i^0)$ are the coordinates of the N_i-O_i vector in the laboratory fixed frame.

The rotational dynamics of each molecule leads to a time dependence of the angles $(a_i^0\, \beta_i^0\, \gamma_i^0)$. If we assume that the rotational motion is fast compared to the duration of the exchange interaction (i.e., $\tau_R \ll \tau_1$, then it is appropriate to average $D^2_{m'',m'}(a_i^0\, \beta_i^0\, \gamma_i^0)$ in equation (68) over this rotational motion. For uniaxial liquid crystals, the well-known result of such averaging is (see equation (12)):

$$\langle D^2_{m'',m'}(a_i^0\, \beta_i^0\, \gamma_i^0) \rangle = \langle D^2_{m'',0}(a_i^0\, \beta_i^0\, \gamma_i^0) \rangle\, \delta_{m',0}. \tag{69}$$

For convenience, let us consider axially symmetric ordering of the nitroxide molecule, then:

$$\langle D^2_{m'',0}(a_i^0\, \beta_i^0\, \gamma_i^0 \rangle = S\, \delta_{m'',0}, \tag{70}$$

where $S = \langle D^2_{00} \rangle$ is the order parameter. This substitution leads to:

$$Y^{int}_{2,m}(\theta'_i, \phi'_i) = Y^{mol}_{2,0}(\pi/2)\, SD^{2}_{0,m}(\beta\gamma)_{(lab\rightarrow int)} \qquad (71)$$

$$= -(S/2)\, Y_{2,m}(\beta\gamma),$$

where on the right hand side, the subscript (lab → int) is implicit. This equation when substituted into equations (65) and (66, 67) leads to:

$$\langle J \rangle = (4\pi/3)\, J_\sigma (A'/3 - B'/5), \qquad (72)$$

where

$$A' = (1/4\pi)\left[SP_2(\cos\beta) - 1\right]^2 \qquad (73)$$

and

$$B' = -(15/16\pi)\, S^2 \sin^2\beta \cos^2\beta. \qquad (74)$$

We shall now consider some limiting cases of equation (72) that are useful in understanding the HE mechanism in liquid crystals:

(i) $S = 0$. This is the case of an isotropic liquid, and leads to

$$\langle J \rangle_{S=0} = (1/9)\, J_\sigma. \qquad (75)$$

(ii) $S = 1$. The molecules are perfectly ordered and in this case, we have:

$$\langle J \rangle_{S=1} = (1/4)\, J_\sigma \sin^2\beta. \qquad (76)$$

According to this equation (as well as equation (72)) the effective exchange interaction depends upon the angle β, i.e., there will be a range of $\langle J \rangle$ depending on the orientation of the internuclear axis with respect to the nematic director for each collision. For example, equation (76) shows that when the radicals diffuse towards each other along an axis which is perpendicular to the mean director (i.e., $\beta = 90°$, see figure 9a), $\langle J \rangle$ is at its maximum value $(1/4)J_\sigma$. However, when the inter-radical axis lies along the nematic director (i.e., $\beta = 0°$ or $180°$ see figure 9b), $\langle J \rangle = 0$.

Now for convenience, let us average over $\sin^2\beta$ in equation (76) to describe an average collision. Thus, for example, in the nematic phase, the inter-radical axis is randomly oriented with respect to the director, so that

$$\langle \sin^2\beta \rangle = \int_0^\pi d\beta \sin^3\beta \,/ \int_0^\pi d\beta \sin\beta \qquad (77)$$

$$= (2/3).$$

In the S_A phase, the molecules are arranged in layers with the principal diffusion expected to be lateral diffusion in the smectic plane, so that the distribution function is peaked about $\beta = 90°$; in this case,

$$\langle \sin^2\beta \rangle \approx \int_0^\pi d\beta \sin^3\beta\, \delta\left(\beta - (\pi/2)\right) / \int_0^\pi d\beta \sin\beta\, \delta\left(\beta - (\pi/2)\right) \qquad (78)$$

$$= 1.$$

Therefore, when the liquid-crystalline system is cooled from the N to the S_A phase, the average exchange integral for a moderately ordered spin probe could increase somewhat [36].

More precisely, in a smectic phase we must consider the positional order. Thus, the inter-radical

separation vector **r**, in particular its z component (parallel to the nematic director), may be restricted by the non-uniform smectic distribution function $P(z)$ for the location of the radical with respect to the bilayer normal. The translational diffusion in this laboratory frame can become very anisotropic [37] such that collisions for $\mathbf{r} \parallel \mathbf{z}$ are significantly more infrequent than collisions for $\mathbf{r} \perp \mathbf{z}$.

5.1.2. *Dipole-Dipole Interactions and Translational Diffusion.* Besides HE, concentration dependent line broadening can also result from dipole-dipole interactions between the electron spins on neighbouring radicals. Therefore, a correct measurement of ω_{HE} is possible only when the contribution to the linewidth due to dipolar interactions is known [27,28]. This effect can be estimated using the point-dipole results for the dipolar coupling of spins as discussed elsewhere [28]. The dipolar contributions to the linewidth are given by [28,38]:

$$T_2^{-1}(\text{dip}) \approx \hbar^2 \gamma^4 S(S+1)\left[(5N + 8D_M)/24N\right] J^{(0)}(0), \tag{79}$$

where $J^{(0)}(0)$, the zero-frequency spectral density is given by [38,23]:

$$J^{(0)}(0) = (48\pi/15)(4\rho/27dD_T) \tag{80}$$

for a simple diffusive model. The HE contribution to the linewidth, in the strong exchange limit, is (see equation (52)):

$$T_2^{-1}(\text{HE}) = \left[(N - 2D_M)/N\right] 4\pi dD\rho. \tag{81}$$

The quantities appearing in these equations have been defined previously (see equations (52) and (54)). The relative ratio of dipolar to exchange contributions to the spin relaxation can be calculated from equations (79) and (81) as [28]:

$$T_2^{-1}(\text{dip})/T_2^{-1}(\text{HE}) = K_M/(dD_T)^2, \tag{82}$$

where

$$K_M = (2/405)\hbar^2 \gamma^4 S(S+)\left[(5N + 8D_M)/(N - 2D_M)\right]. \tag{83}$$

Substitution into equations (82) and (83) leads to:

$$T_2^{-1}(\text{dip})/T_2^{-1}(\text{HE}) = 0.3762 \times 10^{-26}/(dD_T)^2. \tag{84}$$

Owing to the greater viscosity of solutions at lower temperatures, the role of $T_2^{-1}(\text{dip})$ becomes more important at lower temperatures. For non-spherical molecules, and for those spin-bearing molecules where the spins are off-centre, there are orientational corrections to the dipolar interactions which have been discussed elsewhere [39]. Furthermore, there are likely to be important effects due to the interaction between radicals and the liquid crystal structure via the pair correlation function (see later).

From equations (79) and (81), we note that the excess linewidth, which is determined by the sum of HE and dipolar contributions, is given by the sum of two terms that depend directly and inversely on the diffusion coefficient D_T. Assuming the temperature dependence of D_T to be Arrhenius-like, the expected temperature dependence of the excess linewidth may be analysed in

terms of the relation:

$$W \equiv \delta - \delta(0) = \left[A \exp(-\Delta E_{act}/k_B T) + B \exp(\Delta E_{act}/k_B T)\right] C, \tag{85}$$

where W denotes the excess peak-to-peak derivative linewidth, and ΔE_{act} is the activation energy for translational diffusion. A and B are two constants that are independent of concentration, and for simplicity, are also taken to be independent of temperature; (however, more generally, they may depend on temperature as discussed later). The concentration dependence is eliminated by considering the derivative dW/dC, which has the dimensions of a rate constant k:

$$k \equiv dW/dC = A \exp(-\Delta E_{act}/k_B T) + B \exp(\Delta E_{act}/k_B T). \tag{86}$$

The ratio of the two terms on the right hand side of this equation represents the relative contributions of HE and dipolar interactions to the linewidth. Using equations (79) and (81), we calculate, for nitroxide radicals,

$$A = 3.31 \times 10^{14}(dD_0) \tag{87}$$

and

$$B = 1.24 \times 10^{-12}/dD_0. \tag{88}$$

In these expressions, D_0 is the pre-exponential factor in the Arrhenius expression for the diffusion coefficient $[D_T = D_0 \exp(-\Delta E_{act}/k_B T)]$.

5.1.3. *Effect of Interaction Potentials and Pair Correlation Functions.* Pedersen and Freed [32] have provided a more general formulation for Heisenberg spin exchange than the earlier work of Eastman et al. [28] on which the analysis described so far was based. The former supplants the earlier theory by (i) allowing for the finite range of the exchange interaction in the expression for τ_1, the lifetime of the exchanging radical pair; (ii) taking account of the interaction potential between radicals and of the liquid structure via the pair distribution function; and (iii) allowing for the successive re-encounters of the same radical pair after they have separated, (i.e., the cage effect in liquids). Here we emphasise the effect of pair correlation functions in the analysis of some data which could not be rationalised on the basis of the simple treatment [40].

The results of the Pedersen-Freed treatment may be summarised by writing the HE frequency as:

$$\begin{aligned} \omega_{HE} &= \left[N/(N - 2D_M)\right](T_2)^{-1}(\mathrm{HE}) \\ &= 4\pi D_T \rho g(J_0 d^2/D, \lambda d)\, p(d_t), \end{aligned} \tag{89}$$

where the symbols have their usual meanings (cf. equation (81); g and p in equation (89) are defined by:

$$g(J_0 d^2/2D, \lambda d) \approx f^* + (\lambda d)^{-1} \ln\left[\left(\frac{J_0 d^2}{4D}\right) \cdot \frac{f^*}{\lambda d} + 1\right] \tag{90}$$

$$p(d_t) \approx (J_0 \tau_1)^2 \Big/ \left[(1 + (J_0 \tau_1)^2)\right], \tag{91}$$

$$\tau_1 \approx \left(d^2/2D(\lambda d)\right)\left[1+(\lambda d)^{-1}\right](f^*)^{-1}\exp\left[-U(d)/k_BT\right] \tag{92}$$

and f^* is a partition function given by:

$$(f^*)^{-1} = d\int_d^\infty dr\, r^{-2}\exp\left[-U(r)/k_BT\right]. \tag{93}$$

In these equations, λ is related to the finite range of the encounter leading to spin exchange (see equation (59), and $U(r)$, the potential of mean force, is related to the pair correlation function $g(r)$ by:

$$\ln g(r) \equiv -U(r)/k_BT. \tag{94}$$

(Note also that J_0 in [32] is one half the J_0 used here.)

We shall now simplify equation (89) to obtain an approximate but useful form for T_2^{-1}(HE). For typical values [nitroxides [33,41]] of $J_0(10^{11}-10^{12}$ rad s$^{-1})$, $d(\sim 7$ Å) and D_T in liquid crystals $(10^{-6}-10^{-7}$ cm^2 s$^{-1})$, the logarithmic term in equation (90), which approximates the correction to τ_2^{-1} in equation (54) due to the finite range of J(r), may be neglected in comparison to f^* Equation (89) then simplifies to:

$$\left[N/(N-2D_M)\right]T_2^{-1}(\mathrm{HE}) = 4\pi\, dD_T(10^{-3}N_A)\,Cf^*(J_0\tau_1)^2/\left[1+(J_0\tau_1)^2\right] \tag{95}$$

which, in the limit of strong exchange becomes

$$\left[N/(N-2D_M)\right]T_2^{-1}(\mathrm{HE}) = 4\pi\, dD_T(10^{-3}N_A)\,Cf^*. \tag{96}$$

It has also been suggested [23] that the effect of pair correlation functions on the electron-spin electron-spin dipolar interactions is to replace $J(0)$ in the expression for T_2^{-1}(dip) (see equation (79)) by $(f^*)^{-1}\exp(-U(d)/k_BT)\,J(0)$. With this substitution, equation (79) now becomes:

$$\begin{aligned} T_2^{-1}(\mathrm{dip}) &\approx \hbar^2\gamma_e^4 S(S+1)\left[(5N+8D_M)/24N\right](48\pi/15) \\ &\times (4\times 10^{-3}N_A\,C/27dD_T)(f^*\exp\left(U(d)/k_BT\right)^{-1}. \end{aligned} \tag{97}$$

Using equations (96) and (97), and the Stokes-Einstein expression for the diffusion coefficient, it can be shown that:

$$\begin{aligned} k = (dW/dC) &\equiv (2/\sqrt{3}\,\lambda_e)\,d\left\{T_2^{-1}(\mathrm{HE})+T_2^{-1}(\mathrm{dip})\right\}/dC \\ &= A''f^*(T/\eta)+B''\left[f^*\exp\left(U(d)/k_BT\right)\right]^{-1}(\eta/T), \end{aligned} \tag{98}$$

where

$$A'' \approx 4.85\times 10^{-3} \tag{99}$$

and

$$B'' \approx 8.48\times 10^{4}. \tag{100}$$

Alternatively, we may substitute the Arrhenius expression for D_T into equations (95) and (96) and

(97) to obtain:

$$k = (2/\sqrt{3}\,\gamma_e)\, d\left[T_2^{-1}(\mathrm{HE}) + T_2^{-1}(\mathrm{dip})\right]/dC \qquad (101)$$
$$= A' f^* \exp(-\Delta E_{act}/k_B T) + B' \left[f^* \exp\{U(d)/k_B T\}\right]^{-1} \exp(\Delta E_{act}/k_B T),$$

where A' and B' have the same values as A and B given by equations (89) and (90). In equations (98) and (101), f^* is temperature dependent (see equation (93)).

Some examples of the application of HE in obtaining (microscopic) translational diffusion rates are now shown. Figure 10 shows the variation of the excess linewidth W with temperature and concentration for perdeuteriated tempone-d_{16} in 6OCB-8OCB. At a given temperature, k was obtained by performing a linear regression analysis on the W versus C data. A plot of k versus temperature, shown in figure 11 for perdeuteriated tempone-d_{16} in 6OCB-8OCB, was then fitted to equation (88), and gives D_0 and ΔE_{act} directly. Diffusion constants thus obtained for some systems are shown in table 6. [In cases where viscosity data are available, the more general expression (equation (98)) has proved useful.]

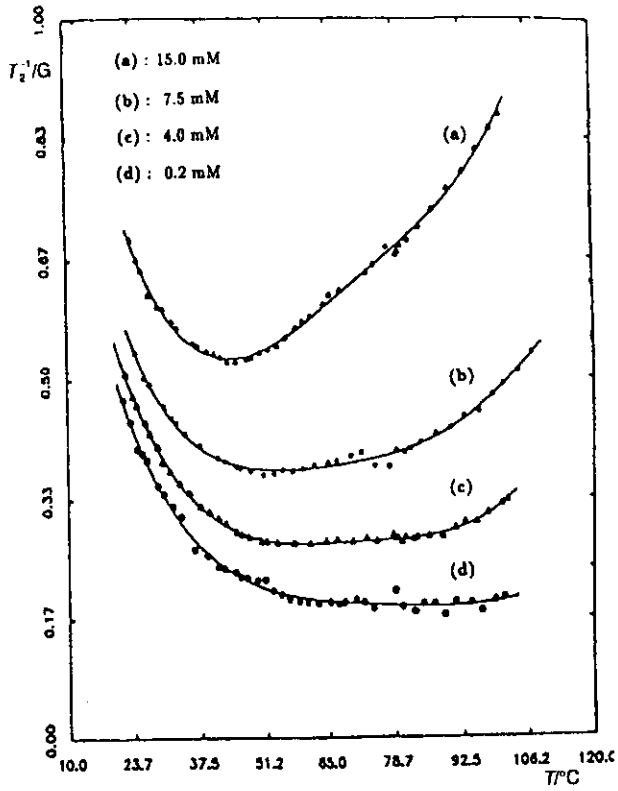

Figure 10. Perdeuteriated tempone in 6OCB-8OCB: Excess linewidth at different concentrations (as indicated) and temperatures. (From [25]).

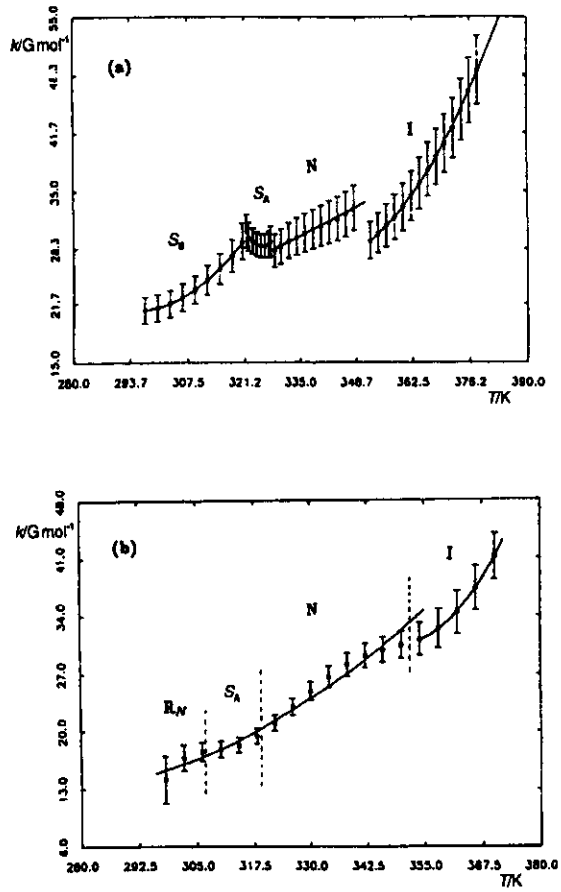

Figure 11. Perdeuteriated tempone in (a) 4O.6 and (b) 6OCB-8OCB, showing the variation of k with temperature. The lines through the data denote our fits using equation (88). (From [25]).

5.2. MACROSCOPICS: DYNAMIC IMAGING OF DIFFUSION

The measurement of diffusion coefficients by ESR imaging is an application that we refer to as dynamic imaging [43]. It involves two stages. A sample is prepared with an inhomogeneous distribution of spin probes along a given direction. The ESR imaging method is first utilised to obtain the (one dimensional) concentration profiles at several different times. The imaging method is based on the use of a magnetic field gradient, such that at each spatial point there is a different local resonant frequency. A typical ESR spectrum from imaging concentration profiles is shown in figure 12 [42]; also shown are the concentration profiles in figure 13. With the passage of time, this inhomogenous distribution will tend to a homogeneous distribution via translational diffusion. The second stage is to fit the time dependent concentration profiles to the diffusion equation in order to obtain the diffusion coefficient. We have shown [43] that the analysis is greatly improved by studying the spatial Fourier transform of the concentration profiles.

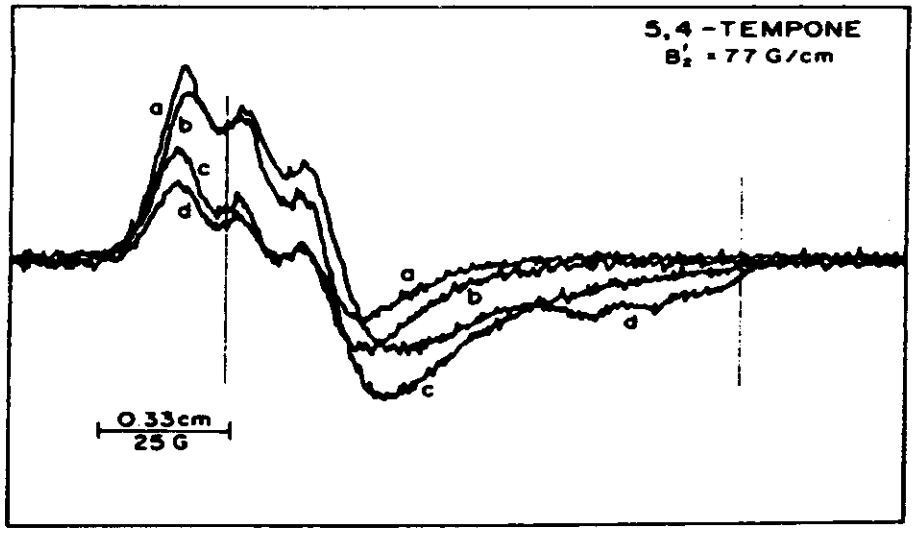

Figure 12. Concentration profiles for perdeuteriated tempone diffusing in the nematic phase of 5,4 at 300K, deconvoluted using the Fourier transform technique discussed by Hornak et al. [42]. The three curves were recorded at different relative times (a) 220 ms, (b) 970 ms and (c) 1.56 s after the start of diffusion. The broken lines are linear least squares fits to the data, with D_T equal to (a) 9.32×10^{-2}, (b) 0.142, and (c) 0.93 cm^2. (From [42]).

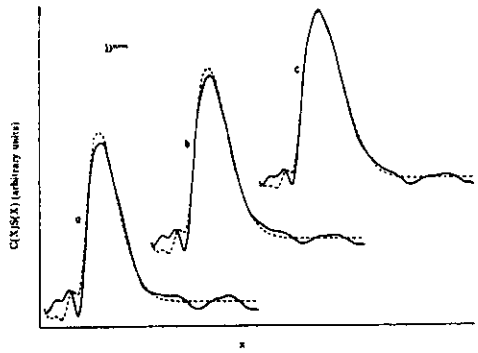

Figure 13. Series of ESR spectra of tempone in the nematic phase of 5,4 from imaging concentration profiles along the X axis of the cavity. The concentration profile is from tempone diffusion from a point source at the left of the spectrum in a direction parallel to the axis of alignment. The spectra were collected at different relative times following the start of diffusion: (a) 0 s, (b) 3.1×10^4 s, (c) 2.1×10^5 s, and (d) 5.0×10^5 s. (From [42]).

The one dimensional diffusion equation (cf. equation (8) in Chapter 4) in Fourier transform or k space is given by

$$\ln C_1 - \ln C_0 = -4\pi^2 D_T k^2 \Delta t, \tag{102}$$

where $\Delta t = t_1 - t_0$ is the time difference between two measurements, and D_T is the lateral diffusion coefficient. To obtain the concentration profile $C(k, t_i)$ at a given time in k space we deconvolute the gradient-on spectrum with the gradient-off spectrum utilising the convolution theorem in Fourier space:

$$C(k, t_i) = I_g(k, t_i)/I_0(k), \tag{103}$$

where $I_g(k)$ is the Fourier transformed gradient-on spectrum and $I_0(k)$ is a Fourier transformed gradient-off spectrum. The diffusion coefficient D_T is determined by the method described elsewhere [43]. In summary, since the samples we have used are well approximated by a gaussian initial spin probe distribution:

$$C(x) = (C_0\sqrt{2\pi}\,\delta)\exp(-x^2/2\delta^2) \tag{104}$$

the ln of the concentration profile in k space may be written as

$$\ln C_i = a(t_i)\,k^2, \tag{105}$$

where

$$a(t_i) = -2\pi^2\delta^2 - 4\pi^2 D_T t_i.$$

Thus, by plotting C_i with respect to k^2 we obtain the slope $a(t_i)$. The $a(t_i)$'s are related to each other by the diffusion equation (see equation (102))

$$a_i - a_j = -4\pi^2 D_T(t_i - t_j). \tag{106}$$

Thus a plot of a_i's with respect to t_i yields D_T. We could estimate the half width at half maximum, Γ, of the gaussian concentration distribution from

$$\Gamma(t_i) = \frac{1}{\pi}\sqrt{-a_i \ln 2} \tag{107}$$

at a given time t_i. The width of the gaussian profiles were about 0.5 mm at the beginning of the measurement. An example of diffusion coefficients measured by this method is shown in figure 14 and table 5; more examples are given in [43,44] and in Chapter 13.

Note added in proof. The dynamic imaging of diffusion ESR method has recently been generalised to provide spatial resolution of the full ESR spectrum. This has enabled simultaneous measurement of the microscopic D_T by Heisenberg exchange and the macroscopic D_T by DID-ESR on a lyotropic liquid crystal [45]. The macroscopic value was found to be somewhat larger.

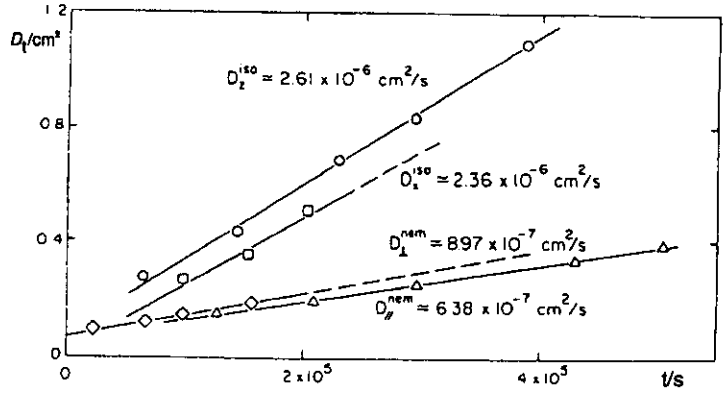

Figure 14. D_T versus time for tempone in 5.4. The phase and direction of diffusion are (a) ○, isotropic and Z axis; (b) □, isotropic and X axis; (c) △, nematic and parallel, and (d) ◇, nematic and perpendicular. The solid lines are fits to the data, with D_T equal to (a) 2.61×10^{-6}; (b) 2.36×10^{-6}; (c) 8.97×10^{-7}, and (d) 6.83×10^{-7} cm^2 s^{-1}. The calculated value of $D_T^{\parallel}/D_T^{\perp}$ is 0.71. (From [42]).

We wish to acknowledge financial support for this work by NSF Grant No. DMR 8901718.

References

[1] Freed, J. H. and G.K. Fraenkel, G. K. (1963) J. chem. Phys., **39**, 326.
[2] Polnaszek, C. F., Bruno, G. V. and Freed, J. H. (1973) J. chem. Phys., **58**, 3185.
[3] Lin, W. J. and Freed, J. H. (1979) J. phys. Chem., **83**, 379.
[4] Goldman, S. A., Bruno, G. V., Polnaszek, C. V. and Freed, J. H. (1972) J. chem. Phys., **56**, 716.
[5] Polnaszek, C. F. and Freed, J. H. (1975) J. phys. Chem., **79**, 2283.
[6] Freed, J. H. (1979) Multiple Electron Resonance Spectroscopy, M. Dorio and J. H. Freed (eds.), Plenum, New York, Chap. 3.
[7] Rose, M. E. (1957) Elementary Theory of Angular Momentum, Wiley, New York.
[8] Luckhurst, G. R. and Zannoni, C. (1977) Proc. R. Soc. Lond. A., **353**, 87.
[9] (a) Freed, J. H. (1976) Spin Labeling: Theory and Applications, L. J. Berliner (ed.), Academic, New York, Chap. 3; (b) Freed, J. H. (1987) Rotational Dynamics of Small and Macromolecules, Th. Dorfmuller and R. Pecora (eds.), Springer-Verlag, Berlin, p. 89.
[10] Zager, S. A. and Freed, J. H. (1982) J. chem. Phys., **77**, 3344.
[11] Meirovitch, E., Igner, D., Igner, E., Moro, G. and Freed, J. H. (1982) J. chem. Phys., **77**, 3915.
[12] Gorcester, J., Rananavare, S. B. and Freed, J. H. (1989) J. chem. Phys., **90**, 5764.
[13] Rananavare, S. B., Pisipati, V. G. K. M. and Freed, J. H. (1987) Chem. Phys. Lett., **140**, 255.
[14] Nayeem, A. and Freed, J. H. (1989) J. phys. Chem., **93**, 6539.
[15] Hwang, J. S., Mason, R. P., Hwang, L. P. and Freed, J. H. (1975) J. phys. Chem., **79**, 489.
[16] Hwang, J. S., Rao, K. V. S. and Freed, J. H. (1976) J. phys. Chem., **80**, 1490.
[17] Zager, S. A., Ph.D. thesis, Cornell University (1982).
[18] Nayeem, A., Ph.D. thesis, Cornell University (1986).

[19] Meirovitch, E. and Freed, J. H. (1980) J. phys. Chem., **84**, 2459.
[20] Moro, G. and Nordio, P. L. (1985) J. phys. Chem., **89**, 997
[21] van der Drift, E. Ph.D. thesis, Delft Technical University, Delft, The Netherlands (1985).
[22] Millhauser, G.L. and Freed, J. H. (1984) J. chem. Phys., **81**, 37.
[23] Hwang, L. P. and Freed, J. H. (1975) J. chem. Phys., **63**, 118.
[24] Cladis, P. E. (1981) Molec. Crystals liq. Crystals, **67**, 177
[25] Nayeem, A., Rananavare, S. B., Sastry, V. S. S. and Freed, J. H. (1989) J. chem. Phys., **90**, 5764.
[26] Berner, B. and Kivelson, D. (1979) J. phys. Chem., **83**, 1406
[27] Molin, Y. N., Salikhov, K. M. and Zamaraev, K. I. (1980) Spin Exchange: Principles and Applications in Chemistry and Biology, Springer Verlag, New York.
[28] Eastman, M. P., Kooser, R. G., Das, M. R. and Freed, J. H. (1969) J. chem. Phys., **51**, 2690.
[29] (a) Bales, B. L., Swenson, J. A. and Schwartz, R. N. (1974) Molec. Phys., **28**, 143; (b) Jones, L. L. and Schwartz, R. N. (1981) Molec. Phys., **43**, 527.
[30] (a) Freed, J. H. (1966) J. chem. Phys., **45**, 3452; (b) Freed, J. H. (1967) J. phys. Chem., **71**, 38; (c) Plachy, W. and Kivelson, D. (1967) J. chem. Phys., **47**, 3312; (d) Stillman, A. E. and Schwartz, R. N. (1976) J. Magn. Reson., **22**, 269.
[31] This is the conventional form for the lifetime of reacting pairs. It is based upon rewriting $(\tau_1^c)^{-1} \simeq 4\pi D_T d/\Delta V$, where ΔV is the reaction volume. Early theories arbitrarily defined ΔV as the total volume swept by the interacting pair, i.e., $(4/3)\pi d^3$, but detailed studies [32] have shown that $\Delta V \approx 4\pi d^2 \Delta r_j$, which is the annular volume of the contact region, i.e., $J(r)$ equals J_0 from d to $d + \Delta r_j$, and is zero otherwise. This yields $\tau_1^c = d\Delta r_j / D_T$.
[32] (a) Freed, J. H. and Pedersen, J. B. (1976) Adv. Magn. Reson., **8**, 1; (b) Freed, J. H. (1977) Chemically Induced Magnetic Polarization", L. T. Muus et al. (eds.), D. Reidel, Dordrecht-Holland.
[33] Berner, B. and Kivelson, D. (1979) J. phys. Chem., **83**, 1406.
[34] Zientara, G. P. and Freed, J. H. (1979) J. phys. Chem., **83**, 3333.
[35] Atherton, N. M. and Shohoji, M. C. B. (1983) J. Chem. Soc., Faraday, Trans., **79**, 1243.
[36] This assumes that the order parameter S for the spin probe is the same in the N and S_A phases. In fact, however, the spin probes are known to undergo expulsion from ordered to disordered regions as smectic layers begin to form.
[37] Chu, K. S., Ailawadi, N. K. and Moroi, D. S. (1977) Molec. Crystals liq. Crystals, **38**, 45.
[38] Abragam, A. (1961) The Principles of Nuclear Magnetism, Oxford University Press, Oxford.
[39] Belorizky, A. and Gallice, A. (1975) J. Phys. (Paris) **36**, 991.
[40] These corrections are related to equilibrium properties of the fluids. Additional corrections due to hydrodynamic flow discussed by PF [J.B. Pedersen and J.H. Freed, (1975) J. chem. Phys., **62**, 1790] are not considered here.
[41] Leniart, D. S., Connor, H. D. and Freed, J. H. (1975) J. chem. Phys., **63**, 165.
[42] Hornak, J. P., Moscicki, J. K., Schneider, D. J. and Freed, J. H. (1986) J. chem. Phys., **84**, 3387.
[43] (a) Cleary, D., Shin, Y.-K., Schneider, D. J. and Freed, J. H. (1988) J. Magn. Reson., **79**, 474; (b) Moscicki, J. K., Shin, Y.-K. and Freed, J. H. (1991) "EPR Imaging and In Vivo EPR", G. Eaton, S. Eaton and K. Ohno (eds.), CRC Press, Chap. 19.
[44] Moscicki, J. K., Shin, Y.-K. and Freed, J. H. (1993) J. chem. Phys., **99**, 634.
[45] Shin, Y.-K., Ewert, U., Budil, D. and Freed, J. H. (1991) Biophys. J., **59**, 950.